



Minnesota State University, Mankato
Cornerstone: A Collection of Scholarly
and Creative Works for Minnesota
State University, Mankato

All Theses, Dissertations, and Other Capstone
Projects

Theses, Dissertations, and Other Capstone
Projects

2020

Experimental Studies of Interfacial Behavior of Contact System During Liquid Mediated Rough Surfaces Separation

Nhat Le

Minnesota State University, Mankato

Follow this and additional works at: <https://cornerstone.lib.mnsu.edu/etds>

 Part of the [Tribology Commons](#)

Recommended Citation

Le, N. (2020). Experimental studies of interfacial behavior of contact system during liquid mediated rough surfaces separation [Master's thesis, Minnesota State University, Mankato]. Cornerstone: A Collection of Scholarly and Creative Works for Minnesota State University, Mankato. <https://cornerstone.lib.mnsu.edu/etds/998/>

This Thesis is brought to you for free and open access by the Theses, Dissertations, and Other Capstone Projects at Cornerstone: A Collection of Scholarly and Creative Works for Minnesota State University, Mankato. It has been accepted for inclusion in All Theses, Dissertations, and Other Capstone Projects by an authorized administrator of Cornerstone: A Collection of Scholarly and Creative Works for Minnesota State University, Mankato.

Experimental Studies of Interfacial Behavior of Contact System during Liquid Mediated Rough Surfaces Separation

by
Nhat Le

A Thesis Submitted in Partial Fulfillment of the
Requirements for the Degree of
Masters of Science
In
Mechanical Engineering

Minnesota State University, Mankato
Mankato, Minnesota
(May 2020)

Date 04/07/2020

Experimental Studies of Interfacial Behavior of Contact System during Liquid Mediated Rough Surfaces Separation

Nhat Le

This thesis has been examined and approved by the following members of the student's committee.

Dr. Shaobiao Cai, Advisor

Date

Dr. Jin Y. Park, Committee Member

Date

Dr. Matthew P. Simones, Committee Member

Date

ACKNOWLEDGMENTS

I express my gratitude and appreciation to my advisor Dr. Shaobiao Cai for his patient guidance, consistent support, encouragement and enthusiasm which allowed me to advance and for providing an optimal environment for conducting research and thanking him for giving me this opportunity to work with him. I would equally like to thank my committee members: Dr. Jin Y Park and Dr. Matthew P. Simones for their insightful suggestions and guidance in conducting this research. I would like to thank Mr. Kevin Schull for providing a great environment for accompanying research in the laboratory. Lastly, I would like to thank my parents and my girlfriend for their continued support for helping me to achieve my objectives.

Experimental Studies of Interfacial Behavior of Contact System during Liquid Mediated Rough Surfaces Separation

Nhat Le

Masters of Science in Mechanical Engineering

Minnesota State University, Mankato

May 2020

ABSTRACT

In the applications related to liquid-solid interface, their operation could be affected by the properties of the interface especially the applications that have infinitesimal interaction force at the interface surface and high interaction velocity. This study provides real time dynamic force measurement in separation process along with the real time image acquisition to explain the deviation between theoretical and experimental methods. The experimental design, setup and initial conditions for experiment are described in detail for further study related to liquid separating force. The simulation model is created to apply the theoretical model in prediction of meniscus force for different initial conditions. The characteristics of solid liquid interface in static and dynamic state are showed in the study with visual demonstration, and how they can affect the experimental results is presented.

The experiments showed that, in the static state, the evaporation will change the geometric parameters such as the contact angle, the vertical radius or the horizontal radius of liquid bridge, and the change of geometric parameters lead to the change of meniscus force. The analytical or models also showed that the change of maximum separation force caused by volume mass deviation and minimum distance deviation is more significant than that caused by contact angle deviation for the liquid with receding contact angle under 40° . The deviation of maximum separation force was not observed in the experiments with different roughness. In the experiments of different liquid with the same volume, the maximum separation force reduces with the reduction of surface tension if the receding contact angle is similar. The experiment can be conducted with the same liquid on different surface coating (non-wetting coating, nano-textured surfaces) to investigate the effect of hydrophobic contact to meniscus force.

Table of Contents

1. Introduction	1
2. Objectives	9
3. Numerical Study	9
3.1. <i>Liquid bridge model</i>	9
3.2. <i>Liquid bridge simulation for system design</i>	13
4. Experimental Approaches and Design	17
4.1. <i>Approaches</i>	17
4.2. <i>Motor sizing and positioning slide selection</i>	19
4.3. <i>Motor control and real time graphic interface design</i>	20
4.4. <i>Weight balance data reading.</i>	22
4.5. <i>Motorized position slide design</i>	25
4.6. <i>Sample design</i>	26
4.7. <i>Slide position calibration</i>	27
4.8. <i>Final apparatus system</i>	28
4.9. <i>Image analysis process</i>	30
5. Experiment Procedure	32
6. Experiment Testing and Results.	34

6.1. Process examination	34
6.2. Liquid drop analysis	37
6.3. Force analysis of water in static state	39
6.4. Force analysis of glycerol in static state	42
7. Comparison Studies of Design Parameters	45
7.1. Water and design parameters	46
7.1.1. Effect of surface roughness preparations	46
7.1.2. Effect of volume/mass	54
7.1.3. Effect of minimum distance	55
7.2. Glycerol and design parameters	56
7.2.1. Effect of surface roughness preparations	56
7.2.2. Effect of volume/mass	63
7.2.3. Effect of minimum distance	64
7.3. Comparison of water and glycerol	65
8. Conclusion suggestion for future work	69
8.1. Conclusion	69
8.2. Suggestion for future work	71

9. References 72

Appendices.....75

1. Introduction

The solid - liquid interface can be found in many applications with moving liquids such as lubricant in gear box, fuel in engine, liquid in piping system especially in valve operation. The interactions in the solid - liquid interface is more significant in the application with lower load and faster separation time especially in nano/micro devices. Some such applications and devices can be found in the magnetic storage application, digital micromirror devices, and diesel fuel injectors. The subject of liquid mediated separation has been studied and presented in the literature. Cai and Bhushan [1] presented the analyses for a fundamental understanding of the physics of the separation process and insight into the relationships between meniscus and viscous forces. The liquid mediated contacts were simplified into two simple cases: flat-on-flat and sphere-on-flat. Bhushan [2] provided the introduction of liquid-mediated contact and the basic theories to form the fundamental calculations of liquid-solid interface.

The experimental studies have primarily focused on the effect on adhesive forces of factors such as the size of the surfaces, liquid properties (surface tension, contact angle, and viscosity), and operating conditions (including temperature, humidity, and velocity). The effect of humidity on adhesion was studied by McHaffie and Lenher [3]. They showed that the thickness of the film and adhesion both increase with an increase in humidity. McFarlane and Tabor [4] conducted quantitative studies on adhesion due to liquid film through a number of experiments. They observed that with a clean hard surface in dry air, adhesion is negligibly small; however, adhesion is appreciable in moist air. Similar observations of the effect of humidity on adhesion have been made by Miyoshi et al. [5].

L.Wang et. al. [6] investigated a dynamic separation process of a sphere from a flat and sphere from sphere with an intervening liquid meniscus under constant applied force. For each case the meniscus and viscous force are considered to account for the adhesion force in the separation processes and compared with the dominated adhesion force in the process. And it has been found that the separation time is longer for sphere-on-sphere for same limitations. Popov [7] studied the stick-slip behavior of liquid-mediated contacts. It was observed that the mechanical properties of the liquid menisci changed the amplitude and period of the stick-slip phenomena, which indicated that substantial change may occur depending on the size and properties of the liquid meniscus. Since adhesion has a significant effect on the operation accuracy of devices like MEMS/NEMS, it should treat carefully [8] [9].

In [10], bulk motion of a liquid bridge between two nonparallel identical solid surfaces undergoing multiple loading cycles (compressing and stretching) was investigated numerically and experimentally. The study it was shown that the magnitude of the motion (in one loading cycle) increases after each loading cycle, if the contact lines depin only on the narrower side of the bridge during compressing and only on the wider side during stretching (asymmetric depinning). Whereas, depinning on both sides of the bridge (symmetric depinning) reduced the magnitude of bridge motion in each cycle under cyclic loading.

Surface tension-driven self-alignment is a passive and highly-accurate positioning mechanism that can significantly simplify and enhance the construction of advanced microsystems. M. Mastrangeli et. al. [11] explained statics and dynamics of the self-

aligning action of deformed liquid bridges through simple models and experiments, and all fundamental aspects of surface patterning and conditioning, of choice, deposition and confinement of liquids, and of component feeding and interconnection to substrates are illustrated through relevant applications in micro- and nanotechnology.

The evaporation of sessile water droplets on hydrophobic surfaces is a topic which led to numerous investigations. In [12], using a specific device to create liquid bridges within a humid environment and between hydrophobic surfaces, values of geometrical parameters, namely the volume, the exchange surface and contact angles of liquid bridges as a function of the drying time have been evaluated for different temperatures and a fixed relative humidity. This suggests that even in the case of a liquid contained between locally hydrophobic regions, a similarity or a pinning can occur during drying, leading to classic concave menisci shapes observed in the case of hydrophilic contacts.

In [14], surface properties are investigated in evaporating and non-evaporating conditions. A capillary bridge between two large plates (similar to a Hele-Shaw cell) is considered. The temporal evolution of surface forces and mass transfers due to evaporation of the liquid are measured. The force depends on surface properties of the substrate. It is adhesive in the wetting case and repulsive in the non-wetting case. The force is also shown to depend linearly on the volume of the capillary bridge $F \propto V_0$ and inversely to the height of the bridge. Modelling is performed to characterize both surface force and evaporation properties of the capillary bridge.

The transition of a liquid bridge profile from convex to concave and the associated capillary forces are experimentally studied via particle-particle and particle-plane pairs in [13]. The

results demonstrate that a convex liquid bridge appears at a relatively large water volume and small separation distance, where the capillary force remains approximately constant. As the separation distance increases, the liquid bridge is stretched from convex to concave, and the capillary force initially doesn't change much but increases to the maximum value and then decreases gradually. By combining analytical analysis and experimental data, a framework is proposed for predicting the evolution of liquid bridge profiles.

Zhang et. al. [15] presented a study of dynamic contact angle hysteresis using liquid bridges under cyclic compression and stretching between two identical plates. In study, the partial derivative equation of the liquid volume was used to define the liquid bridge dimension for meniscus force calculation. The experiments were done as well by using a high-resolution motor-controlled linear stage and an accurate image measurement system as shown in Fig.1.

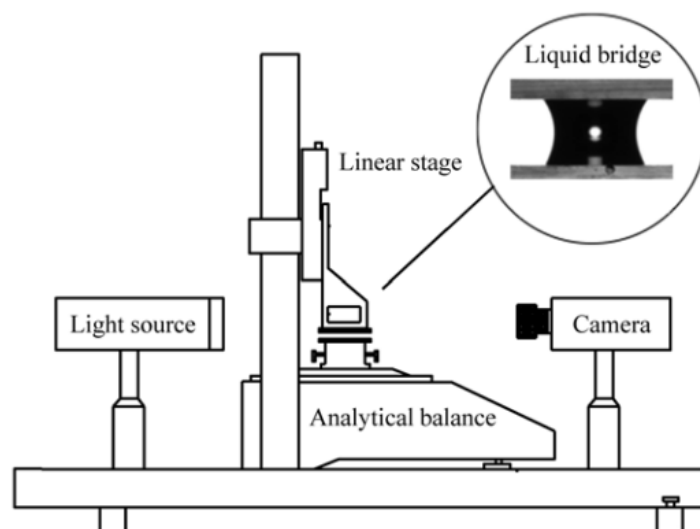


Fig. 1. Schematic representation of the experimental setup [15]

The separation force was measured. However, there is no dynamic presentation of the liquid shape change to demonstrate the correspondence of the change in liquid bridge shape and force during the separation motion. Dhital [16] performed all numerical modeling in order to study the roles of meniscus and viscous forces during flat on flat liquid mediated contacts separation with different liquids or properties, and experimental analysis was made in order to analyze the effect of surface roughness on static contact angle for different liquid properties. The shape change of the liquid bridge during the separation process was captured without the real time force measurement as shown in Fig.2.

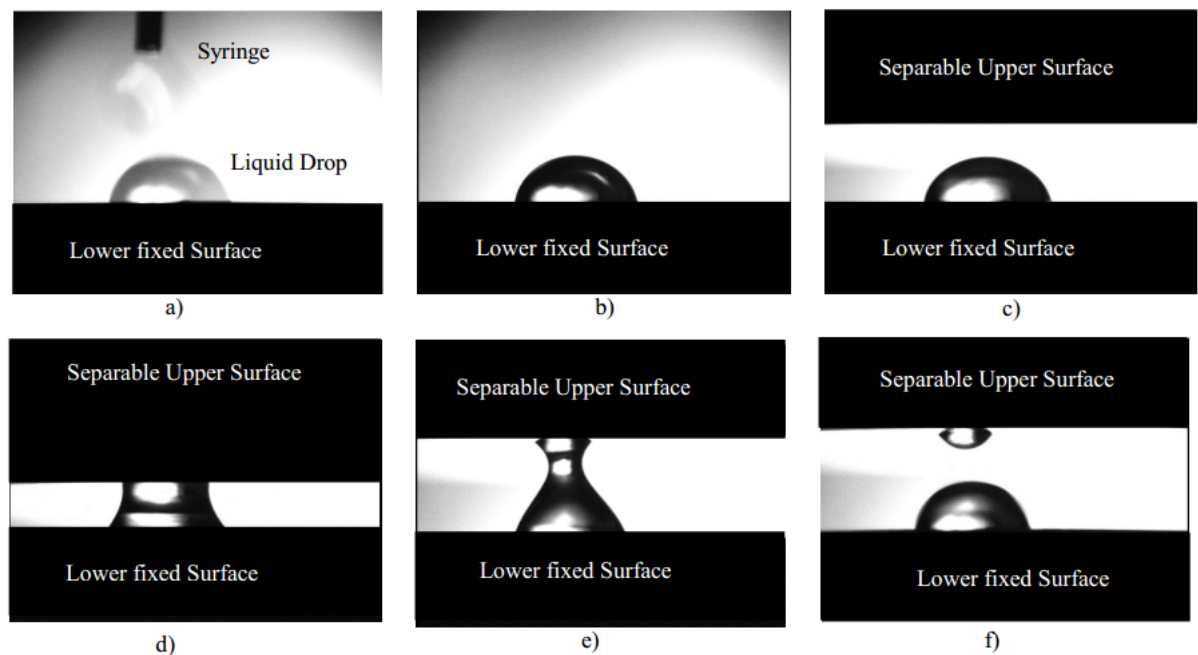


Fig. 2. Series of image in separation process [16]

Adhesive/friction/stiction forces related to liquid – solid interface appear in basic components of many devices. The forces effect the operation of read – write head of hard disk drive, the digital micromirror devices of digital projectors, or the spool valve operation

in fuel injectors. The main components of hard disk drive shown in Fig. 3. includes a magnetic head slider and a metallic disk. The construction of metallic disk is a soft alloy with poor wear and corrosion resistance like Co – Cr. Protective diamond-like carbon (DLC) coatings with a thin lubricant overlay are used to provide low friction, low wear, and corrosion resistance. The appearance of lubricant results in high stiction and friction in start – stop operation of the head slider. The study of liquid – solid interface needs to be considered to limit the affect of liquid – solid adhesive in read – write process of hard disk drive.

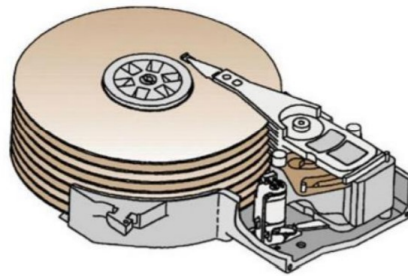


Fig. 3. Schematic of a data processing magnetic rigid disk drive [16].

Digital micromirror device (DMD) is a $12 \mu\text{m}^2$ size mirror with $13 \mu\text{m}$ pitch oscillating at the frequency of 5000 Hz in Fig. 4. A DMD is a pixel in digital projection displays in TV sets, computer projectors, and movie theater projectors. The micro mirror flips backward and forward to reflect or not reflect the light to create or not create the color light on the display corresponding to the digital signal 1 – 0. The mirror is attached on a yoke linked torsional hinge controlled by electrostatic force, and its motion is limited by spring tip contacts at both sides of the yoke. The moisture of ambient environment is condensed

between the contacts of spring tip and landing site and creates the solid – liquid interface.

The stiction forces in the interface directly effects the operation of DMD.

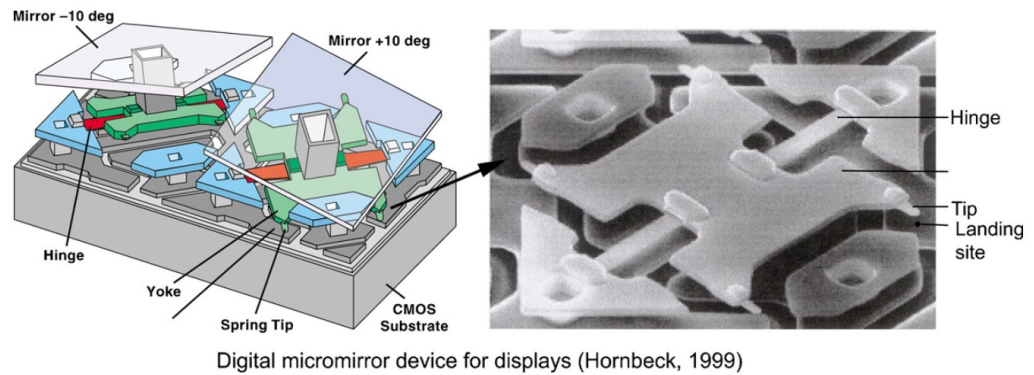


Fig. 4. A DMD device that is affected by stiction force in operation. [1].

Diesel fuel injector is a typical macroscale application that experiences surface stiction during the operation. In Fig. 5., the spool valve of 6.35 mm diameter and the end cap are separated by the engine oil layer of $20\ \mu\text{m}$. The valve is closed to and opened from the end cap by a load 40 N in every $50\ \mu\text{s}$ with a speed of 40 mm/s. During operation, the high-pressure engine oil comes in and pushes piston to move down to inject diesel fuel to engine. The spool valve is always affected by forces caused by solid – liquid interface of engine oil and the end cap. The adhesion issue would impact the reliability of the injector especially in cold weather.

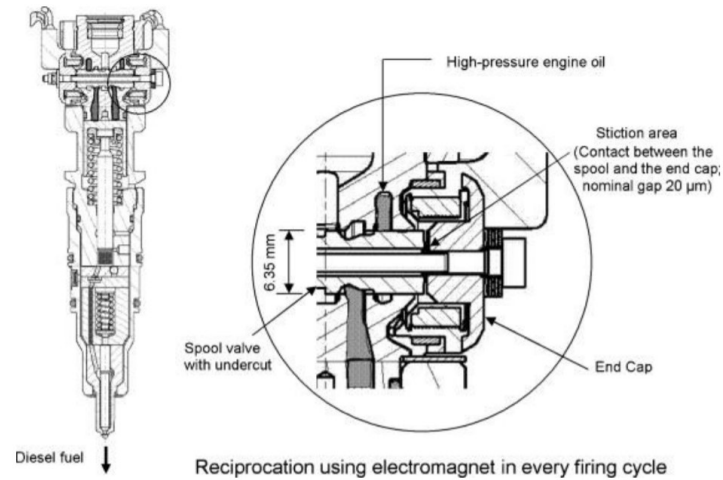


Fig. 5. Schematic of diesel fuel injector which experiences adhesion [16].

This study involved the design and development of an apparatus to investigate the separating forces at real time under various conditions such as surface roughness and different liquids' properties. The affordable motor-controlled slider with an appropriate resolution is designed, and the image analyzing system with a relative accuracy is built by utilizing a laboratory microscope. The equation of liquid bridge volume will be created to calculate the liquid bridge parameters more efficiently and accurately. The system design is also used to study and verify solid liquid interface properties to define stable repeatable experimental process.

2. Objectives

Design and develop an apparatus to investigate the separating forces in real time under various conditions such as surface roughness and different liquid properties.

Investigate and gain insights of the parameters which effect the separation force(s) during dynamic separation processes and verify solid liquid interface properties to define stable repeatable experimental process by using the system designed.

3. Numerical Study

3.1. *Liquid bridge model*

The two contact surfaces are assumed as rigid. The formed meniscus bridge is considered to be mechanical equilibrium and used liquid is incompressible with no thermal effect. The pressure is constant on a vertical cross section plane, whereas it varies along a radial direction through the meniscus bridge during the process of separation. An arc-shaped meniscus is supposed. The volume of liquid mediator is constant during the separation process. The effect of gravity is neglected. The flat on flat case diagram is shown in Fig.6.

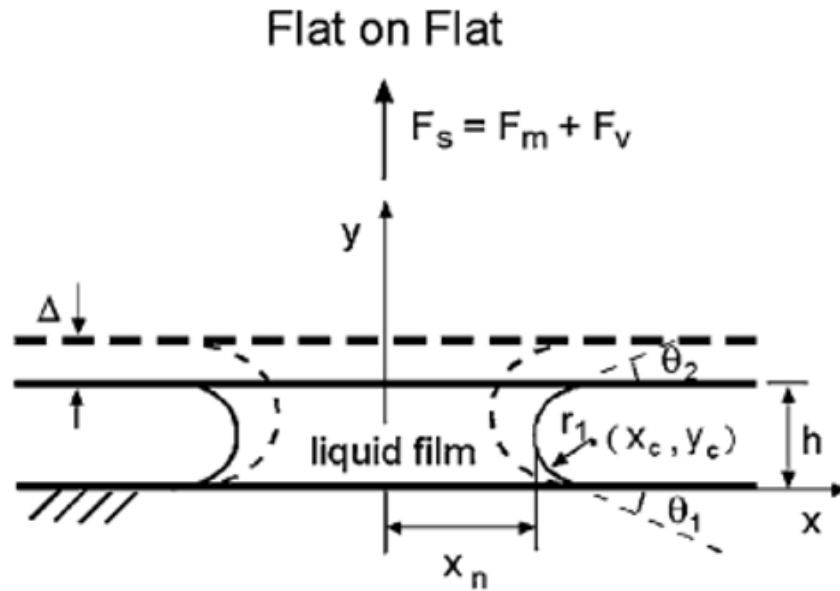


Fig. 6. Diagram of flat on flat case studied in [1].

The meniscus force due to the formation of a meniscus can be obtained by integrating the Laplace pressure over the meniscus area and adding the surface tension effect acting on the circumference of the interface [1]. For the separation of the liquid bridge between two flat surfaces, the meniscus force can be calculated using Eq. (1). The first term in Eq. (1) is the force component caused by the Laplace pressure, and the second term is the force component caused by the surface tension of liquid.

$$F_m = \frac{\pi x_{ni}^2 \gamma}{r_1} + 2\pi \gamma x_{ni} \sin \theta_{1,2} \quad (1)$$

Where x_{ni} is the meniscus radius in the horizontal plane at location i during separation, r_1 is the meniscus radius in vertical plane ($r_1 = h/(\cos \theta_1 + \cos \theta_2)$), γ is the liquid surface

tension, h is the distance of two flat surfaces, $\theta_{1,2}$ is the contact angle of the liquid on the bottom and top surface respectively.

The viscous force can be calculated by multiplying the average pressure difference based on the Reynolds lubrication equation in a cylindrical coordinate system by the meniscus area in the central plane in the direction of separation. Eq. (2) gives the expression for the viscous force at a given distance h (x_{n0} , initial meniscus neck radius).

$$F_v = \frac{3\pi\eta x_{n0}^4}{4t_s} \left(\frac{1}{h^2} - \frac{1}{h_0^2} \right) \quad (2)$$

Where η is the dynamic viscosity, t_s is the time at break point, h_0 is the initial separation distance. Based on experimental evidence, the viscous component of the adhesive force for a liquid mediated contact is given in [2] as Eq. (3).

$$F_v = \frac{\beta\eta}{t_s} \quad (3)$$

Where β is a proportionality constant (dimension of length²), η is the dynamic viscosity of the liquid, and t_s is the time to separate (unstick) the two surfaces.

Theoretical study will be reviewed to create simulation program. The simulation program is created in Matlab and compared with the theory for microscale dimension, $h_0 = 2$ nm, $\gamma = 72$ mN/m, $x_{n0} = 100$ nm, and contact angles $\theta_1 = \theta_2 = 60^\circ$ from [1] as shown in Fig. 7. The meniscus and viscous forces in liquid bridge are analyzed to determine the measurement range for equipment design. The simulation program is used to visualize the separation process and creates plots of the separation forces with different sets of initial

input. The plots are also used to compare experimental and theoretical results with different initial parameters. Assumptions of liquid bridge for numerical calculation are defined for simulation environment. The formula of liquid bridge volume will be created for simulation. For this study, the flat on flat case is chosen between two typical cases flat on flat and sphere on flat. The equation used for separation forces is Eq. (1) and (2).

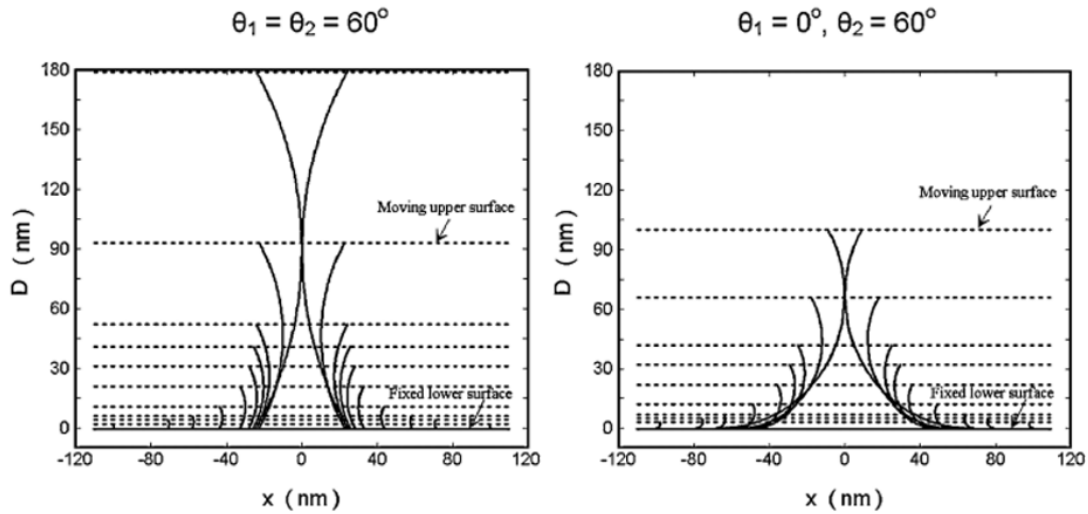


Fig. 7. Meniscus curvatures when separating two parallel flats with initial meniscus height $h_0 = 2$ nm, $\gamma = 72$ mN/m, $x_{n0} = 100$ nm, and contact angles, $\theta_1 = \theta_2 = 60^\circ$ and $\theta_1 = 0^\circ$, $\theta_2 = 60^\circ$ [1]

The model of liquid bridge is shown in Fig. 8. This study will formulate the volume with respect to separation distance the neck radius and formulate the neck radius from the constant volume and height of liquid bridge. The simulation will be applied for water bridge and aluminum surfaces at experimental dimensions: $h_0 = 1$ mm, $\gamma = 72$ mN/m, $x_{n0} = 3$ mm, and contact angles, $\theta_1 = \theta_2 = 60^\circ$, $\eta = 0.89$ cP. This study will determine the appropriate parameters for apparatus design such as range of velocity of upper surface,

range of force that needs to be measured. The meniscus force depends on the bridge radius and the separation distance. The viscous force depends on separation time or separation velocity. The separation velocity will be analyzed to find out the relation between velocity and separation forces to eliminate viscous force in the total separation force.

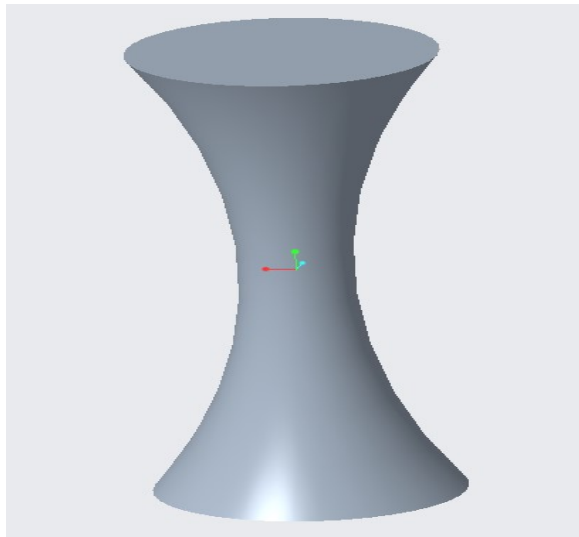


Fig. 8. The 3D model of water bridge between two flat surfaces.

The image of the separation will be captured to observe and measure the dimension of liquid bridge, the change of contact angle and the practical breaking point.

3.2. Liquid bridge simulation for system design

The simulation program is created in Matlab and compared with the theory for the same parameters, $h_0 = 2$ nm, $\gamma = 72$ mN/m, $x_{n0} = 100$ nm, and contact angles, $\theta_1 = \theta_2 = 60^\circ$. The 3D model of liquid bridge is created in Creo to verify the results of the program as shown in Fig.8. Creo uses FEA to calculate volume of the model, and the Creo ensures the accuracy of the volume by limiting the minimum number of the finite elements. The

volume can be changed with different accuracy setup but the variation is under 1% for complicated objects, and even under 0.01% for simpler objects.

By keeping the volume of water bridge constant, the radius of water bridge is calculated when the separation distance is increasing. Fig. 9. shows the diagram of meniscus in separation process with $h_0 = 2$ nm, $\gamma = 72$ mN/m, $x_{n0} = 100$ nm, and contact angles, $\theta_1 = \theta_2 = 60^\circ$ and $\theta_1 = 0^\circ, \theta_2 = 60^\circ$. Fig. 9a) shows the meniscus diagram with certain parameters in literature, and Fig. 9b) shows the meniscus diagram simulated in this study with the same parameters. The results from the simulation are aligned with those in other literature. This simulation will be used as the theoretical baseline for the experimental study.

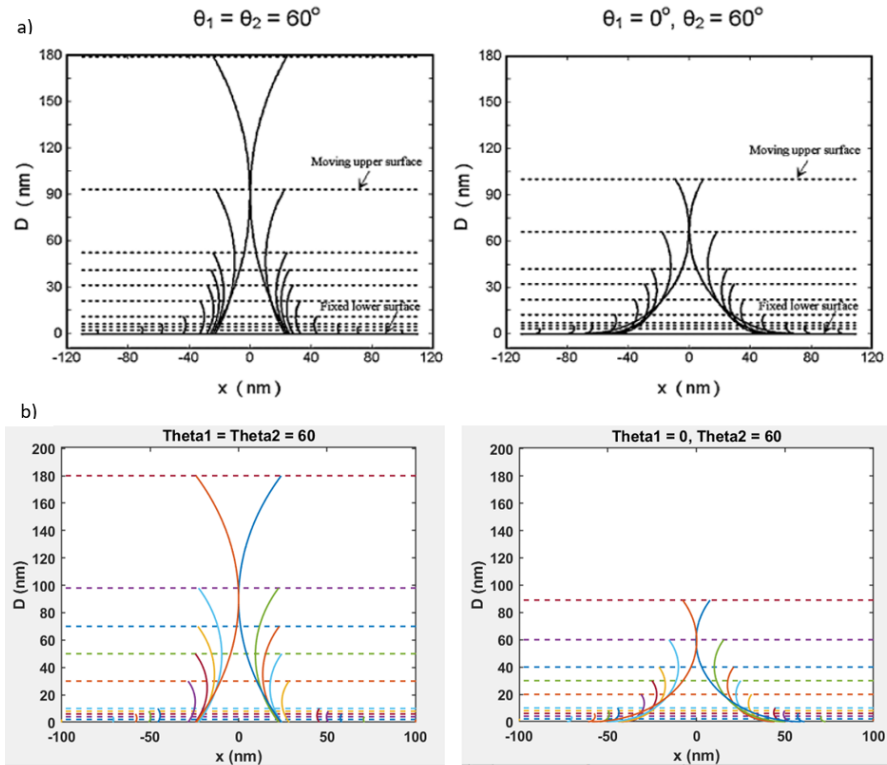


Fig. 9. The diagram of meniscus in separation process. ($h_0 = 2$ nm, $\gamma = 72$ mN/m, $x_{n0} = 100$ nm, and contact angles, $\theta_1 = \theta_2 = 60^\circ$ and $\theta_1 = 0^\circ, \theta_2 = 60^\circ$).

The Eq. (1) and (2) were used to calculate the meniscus force and viscous force respectively, and the results are identical to those in other literature. Fig. 10 shows the forces in separation process in nanoscale. The total adhesive force or the total separation force is the sum of meniscus force and viscous force. The purpose of this is to access the characteristics of separation force by experimental method, but the force in nanoscale is not relevant to conduct experiments. Thus, the initial dimensions of water bridge are scaled up to create measurable separation force. If the initial parameter is set $h_0 = 1$ mm, $\gamma = 72$ mN/m, $x_{n0} = 3$ mm, and contact angles, $\theta_1 = \theta_2 = 60^\circ$, the maximum value of meniscus force is 3.2 mN and the viscous force is inversely proportional to separation time t_s .

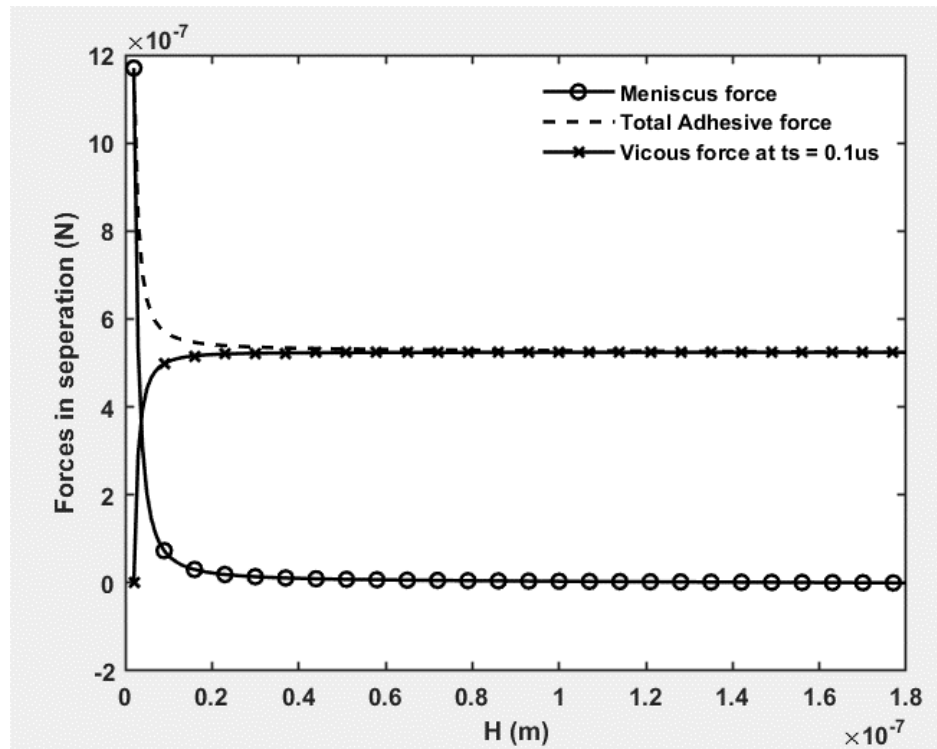


Fig. 10. The plot of forces in separation process. $h_0 = 2$ nm, $\gamma = 72$ mN/m, $x_{n0} = 100$ nm, and contact angles, $\theta_1 = \theta_2 = 60^\circ$, $t_s = 0.1 \mu\text{s}$, $\eta = 0.89$ cP

There are two kinds of force involved in the separation process: meniscus force and viscous force. In order to investigate the properties of each force, one should be eliminated. From the force equations, if the separation time is changed, the meniscus force is unchanged but the viscous force decreases. By increasing the separation time, the viscous force can be eliminated, and Fig. 11 shows meniscus force and viscous forces with $\eta = 0.89$ and $t_s = 0.1$, 0.001, and 0.0001, s respectively. The viscous force can be eliminated by increasing the separation time. The viscous force may be neglected at the separation time of $t_s = 0.1$ since the magnitude is about zero.

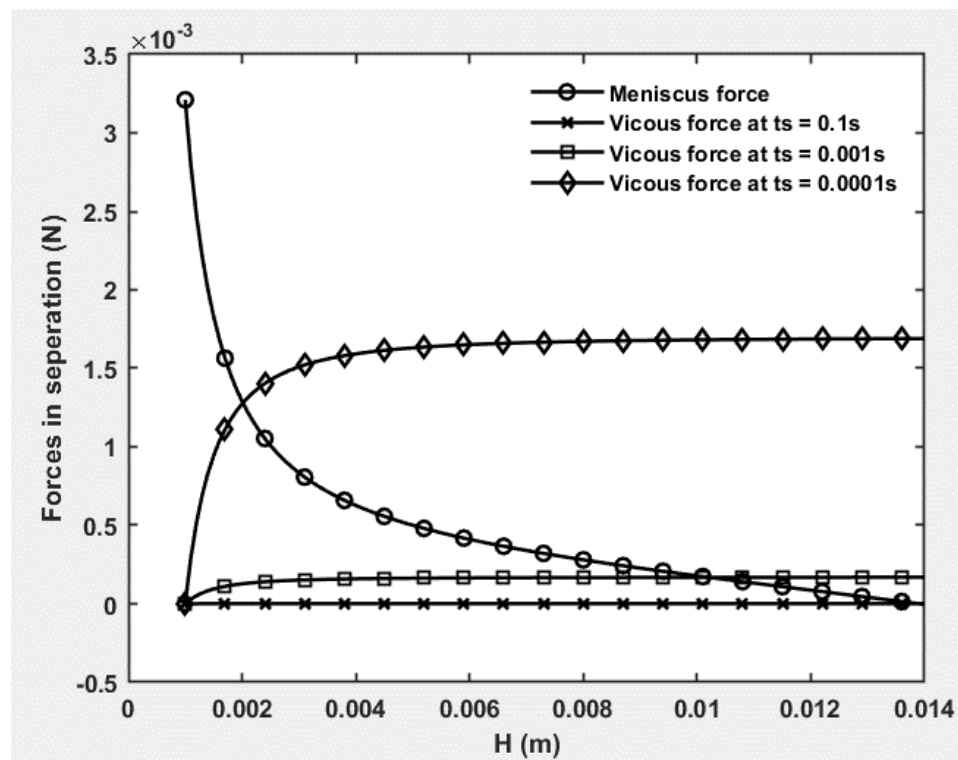


Fig. 11. The plot of meniscus and viscous forces in separation process ($h_0 = 1$ mm, $\gamma = 72$ mN/m, $x_{n0} = 3$ mm, and contact angles, $\theta_1 = \theta_2 = 60^\circ$, $\eta = 0.89$ cP, and $t_s = 0.1$, 0.001 and 0.0001s, respectively).

4. Experimental Approaches and Design

4.1. Approaches

The viscous force can be eliminated by increasing the separation time. In Fig.11, the viscous force is around zero value at the separation time of $t_s = 0.1$. Because the purpose of the experiment is to observe the separation process, the separation time needed to be increased. Furthermore, the assumption of the breaking condition is when the water bridge radius comes to zero, but in practice, the liquid always breaks before the radius comes to zero. Therefore, the actual breaking time must be smaller than in the simulation. The separation time should be increased to compensate for that early breaking, the chosen separation time is $t_s = 20$ s. From the simulation result, the travelling distance before breaking is 13 mm.

A mechanism to control the upper surface's movement to create the liquid bridge needs to be designed. From the theoretical calculation, the maximum velocity for the linear stage is 13/20 mm/s (0.65 mm/s), and the maximum separation force is 3.2 mN. There are two typical actuators for linear motion: hydraulic linear actuator and motor - lead screw mechanism. The hydraulic system shown in Fig.12 requires quite a lot of components to operate such as pressure valve, directional valve, reservoir, filter, motor, pump, and cylinder.

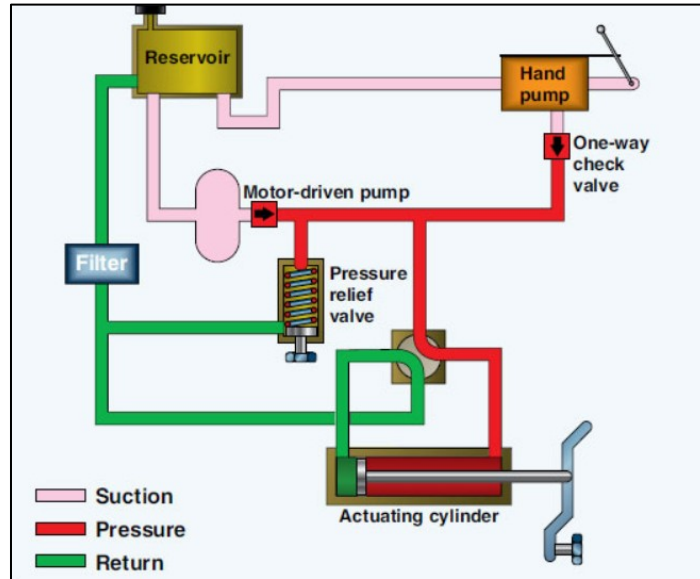


Fig. 12. Hydraulic linear actuator schematic diagram [17]

Motor–lead screw mechanism shown in Fig. 13 only requires three components (motor, ball screw, and sliding actuator) to run. Table 1 shows the comparison of the two mechanisms, and the motor–lead screw system was chosen because it is easy to control, affordable and simple to assemble.

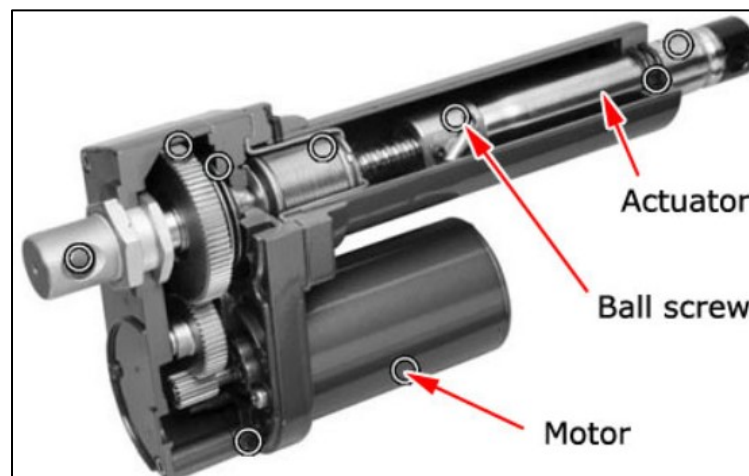


Fig. 13. Motor – lead screw mechanism [18]

Table 1. The comparison table of two typical linear mechanisms

Hydraulic linear actuator	Motorized linear actuator
Complicated system, many components required	Simple system, less component required
Difficult to control	Easy to control
Appropriate for high force application	Appropriate for small to medium force application
High cost	Lower cost

The two main components of motorized linear actuator are a screw nut sliding and a driving motor. There are a lot of options for the driving motor such as DC motor, servo motor, and step motor but DC motor requires encoder for speed control, servo motor is appropriate for position. Step motor is chosen for this application requiring speed and position control. The mechanism of screw sliding and step motor is chosen.

4.2. Motor sizing and positioning slide selection

From the theoretical calculation, the maximum velocity for the linear stage is $13/20$ mm/s – 0.65 mm/s. The typical number of step in stepper motor is 200 step/revolution. In order to distribute velocity 0.65 mm equally in 1 second, the stepper motor needs to run at least 20 step/second for slider to go 0.65 mm. The larger the number of step/second is, the more smoothly the slider runs. Therefore, the maximum resolution of the motor slider system is $0.65/20 = 0.0325$ mm/step. The calculated maximum lead of the lead screw is $0.0325 \times 200 = 6.5$ mm/revolution, and the smaller lead is better. The chosen lead screw has the lead of 1.27 mm. We estimate the load and friction of positioning slide to calculate the acceleration

needed for sizing the power of motor following the formulas in [19]. The torque of chosen step motor (Bipolar Stepper Motor Hybrid Frame Size 23 200 Step 2A 3.2VDC – holding torque 120 Ncm from Digikey) is larger than the calculation to compensate for the estimation. The slide (Positioning Slide, 15 lbs. Static Load Capacity, 1.500" Travel Length) is chosen with a suitable lead and tolerance from McMASTER-CARR. A flexible shaft coupler is used to connect motor and lead screw.

4.3. Motor control and real time graphic interface design

To control the motor, the Arduino is connected to an appropriate power circuit and controlled by computer with Labview interface. In [20], the limit voltage and current of power supply for driver circuit are presented. The connection and pin configuration are described in there. The direction to setup for micro step (increasing the resolution of the motor) is mentioned in there as well. The sample control program is also given to run the motor.

Step motor receives a pulse signal to operate, and its speed is controlled exactly by the frequency of the signal. Step motor will stop if missing the pulse from signal or overload. The overload issue is covered in section 4.2. To control the step motor speed exactly, the frequency of the signal controlling the stepper motor must be as accurate as possible. Labview has an Arduino command that can request Arduino generates a signal with an exact frequency. By this way, the tolerance of the frequency or the speed of the step motor is controlled under 1%.

The RS232 interface and Labview are used to program the interface. The motor control interface and its corresponding VIs are presented in Fig. 14. The input to control the step motor and some unit conversion data are shown in Fig. 14a, and the corresponding VIs are presented in Fig 14b. The “Frequency” input is used to control the speed of the motor. The “Frequency” the “step motor resolution” and the “lead screw’s lead” are used to calculate “sliding speed”. The “distance” is for setting the movement distance of the upper surface. The “distance” is divided by the “sliding speed” to provide the “duration” of the controlling signal. The “Max duration” is the waiting time for the motor to finish its motion before receiving the next input. The “lead screw’s lead” and “step motor resolution” input are used for calculating the “linear resolution” value. The “distance initial” and “set distance initial” button are used to set the value of distance in the program. The “Controlling signal to step motor” block will receive data from the input section and send them to the Arduino board.

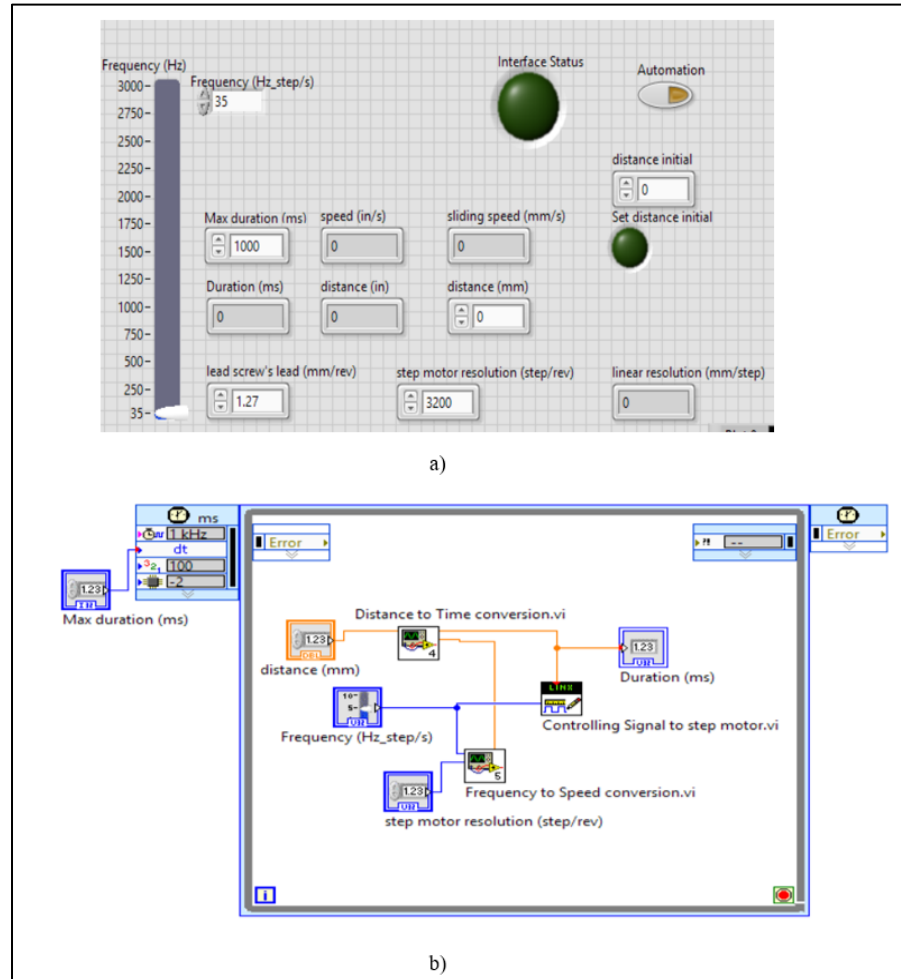


Fig. 14. The input section to control motor: a) Controlling interface of data input, b) Corresponding VIs of data input

4.4. Weight balance data reading

The method to measure a force of a few mN is using a balance with a appropriate range presented in [15] as shown Fig. 1. The balance with an appropriate range has been identified. The balance's brand is Ohaus Explorer 124/AD using loadcell to measure weight. The range, readability, and repeatability of the balance are listed in Table 2. There are the internal, external, and automatic calibration included in the balance. The automatic

calibration allows the balance to calibrate by its internal mass in a certain period or when temperature changes, and the internal mass can be adjusted with the standard mass with the available AutoCal Adjustment option presented in [21].

Table 2. The balance parameters datasheets [22]

Model	EX124	EX224	EX324	EX223	EX423	EX623	EX1103
Automatic Door	EX124/AD	EX224/AD	EX324/AD	—	—	—	—
External Calibration	—	—	—	EX223/E	EX423/E	—	—
Certified Models	EX124N/AD	EX224N EX224N/AD	EX324N EX324N/AD	—	EX423N	—	EX1103N
Capacity (g)	120	220	320	220	420	620	1100
Readability d (g)	0.0001			0.001			
Verification Interval* e (g)	0.001			—	0.01	—	0.01
Class*	I			—	II	—	I
Repeatability std (g)	±0.0001			±0.001			
Linearity (g)	±0.0002			±0.002			

In Ohaus Explorer 124/AD model, the RS232 serial communication is integrated. We used Labview to control and read data from balance RS232 port. The basic parameters for RS232 connection are: baud rate, data bits, parity, stop bits, flow control. The basic parameters need to be set up identically for the weight balance and the computer as shown in Fig. 15, and other parameters are defaults. Fig. 15a) is the setup interface of the weight balance on the computer, and the corresponding VIs are shown in Fig. 15b). The data transferring time of the weight balance has the minimum value, so the transferring time can not be shorter than that minimum. In the computer interface, the time set to read weight balance value needs to be longer than the minimum transferring time of the balance to ensure the reading process does not interrupt the timer of the program. This is because if the reading time set by the computer program is shorter than the time the balance transfers

the data, the program has to wait for the balance finish its process. The reading rate can reach 10 Hz - 10 reading per second.

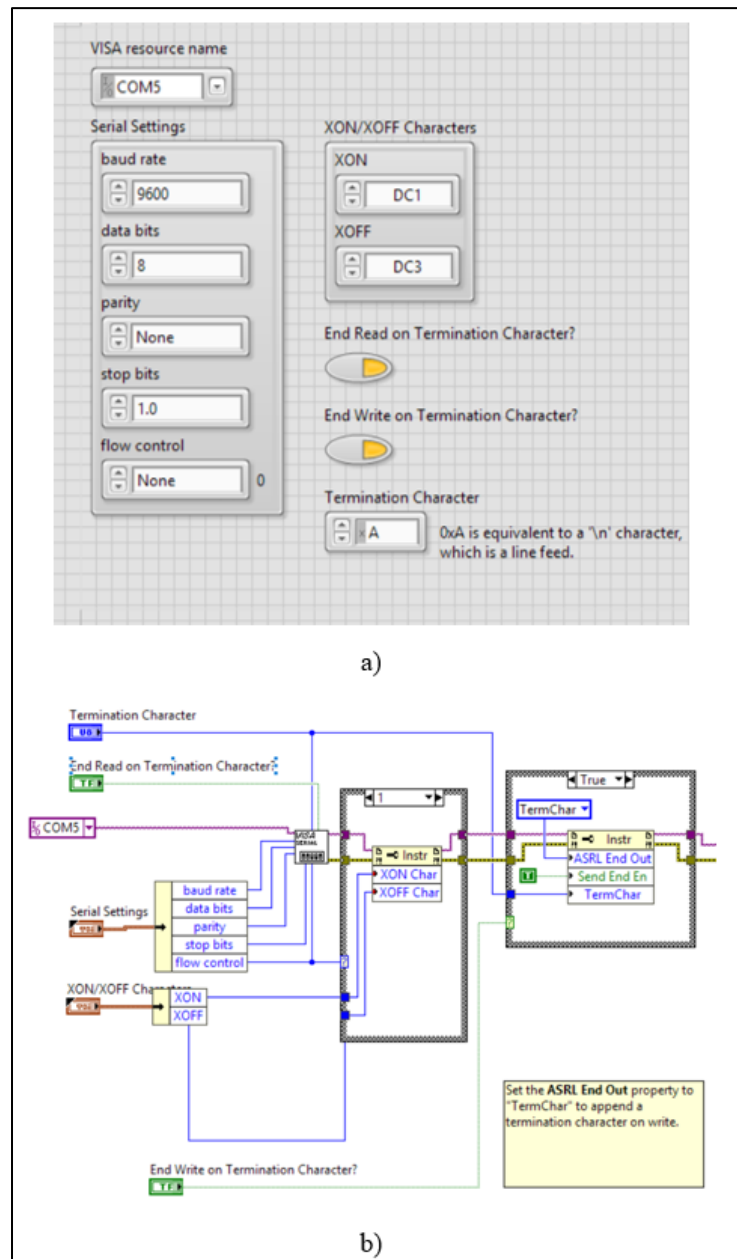


Fig. 15. Program interface for weight balance with communication parameters: a) Controlling interface panel, b) Corresponding VIs diagram

4.5. Motorized position slide design

The main frame is created by 3D printer and the critical parts are made by lathe machine. The geometric tolerances of the lathe machine are smaller than the 3D printer, so the parts created by the lathe are more accurate than those created by 3D printer. There are two requirements for the frame design: the axis of the positioning slide needs to be aligned with the axis of the motor, the two separated surfaces need to be parallel to each other. To make the axes aligned, the positioning slide is fixed on the frame, and the position of motor on the frame is adjustable as shown in Fig. 16.

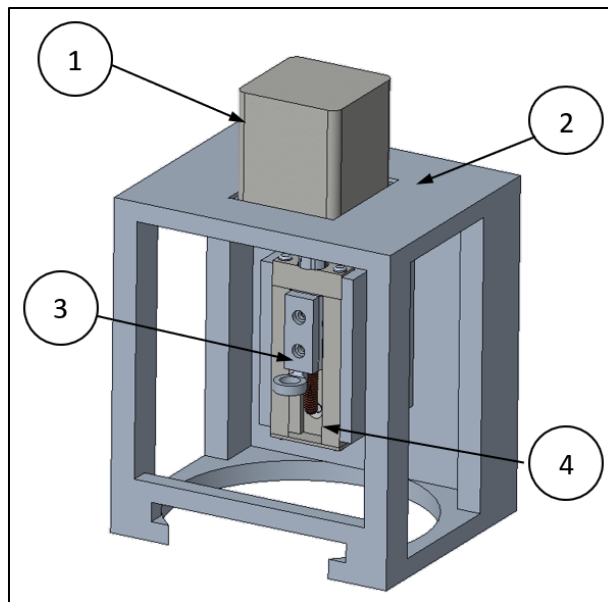


Fig. 16. The final assembly of motorized position slide

- | | |
|-------------------|-----------------------|
| 1 – Step motor | 2 – Main Frame |
| 3 – Sample holder | 4 – Positioning slide |

To make the two separated surfaces are parallel, the two surfaces need to be parallel to the ground datum as shown in Fig. 17. The Inner sleeve and samples are created by lathe to

ensure the parallelism between the alignment surfaces. The top surface is created by the Top sample inserted into the Inner sleeve. The Inner sleeve is fixed to the Sample holder and adjusted to be parallel to the ground. The Top sample is aligned with the sleeve surface to make the top surface parallel to the ground. The bottom surface is place on the weight balance surface adjust to be parallel to the ground.

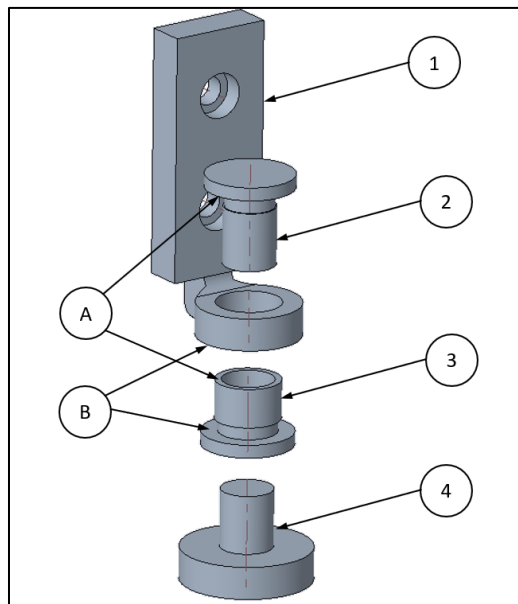


Fig. 17. Sample alignment assembly

1 – Sample holder

2 – Top sample

3 – Inner sleeve

4 – Bottom sample

A - Aligned surfaces between Inner sleeve and Top sample

B - Aligned surfaces between Inner sleeve and Sample holder

4.6. Sample design

The samples are ground by the sandpaper with different grit number such as 240GRIT, 400GRIT, and 600GRIT to create different roughness as shown in Fig. 18. In the grinding

process, the contacting surfaces need to maintain parallel. The samples need to be rotated to make the roughness equal on the whole surface. On the top sample, a groove is created near the sleeve assembled surface to make a good alignment when inserting the sample to the sleeve.

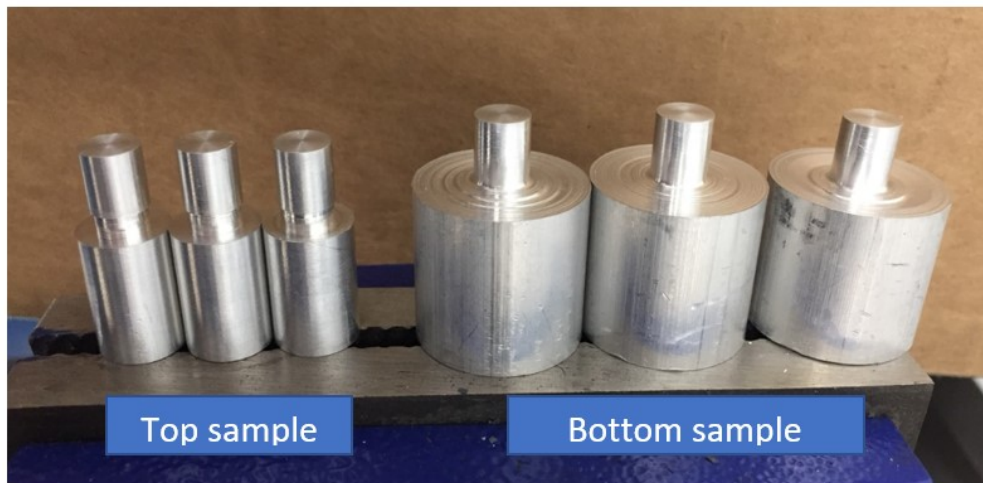


Fig. 18. The samples used in the experiment.

4.7. Slide position calibration

The step motor slide is a non - feedback system, so the position of the slider is calculated from the speed of the motor and the slider's resolution. The position testing shown in Fig. 19 is a setup to check the tolerance of the positioning slide. The dial indicator with the tolerance 0.025 mm is used to measure the displacement of the slider to compare with the position value calculated by the program. The tolerance of the position is ± 0.05 mm.

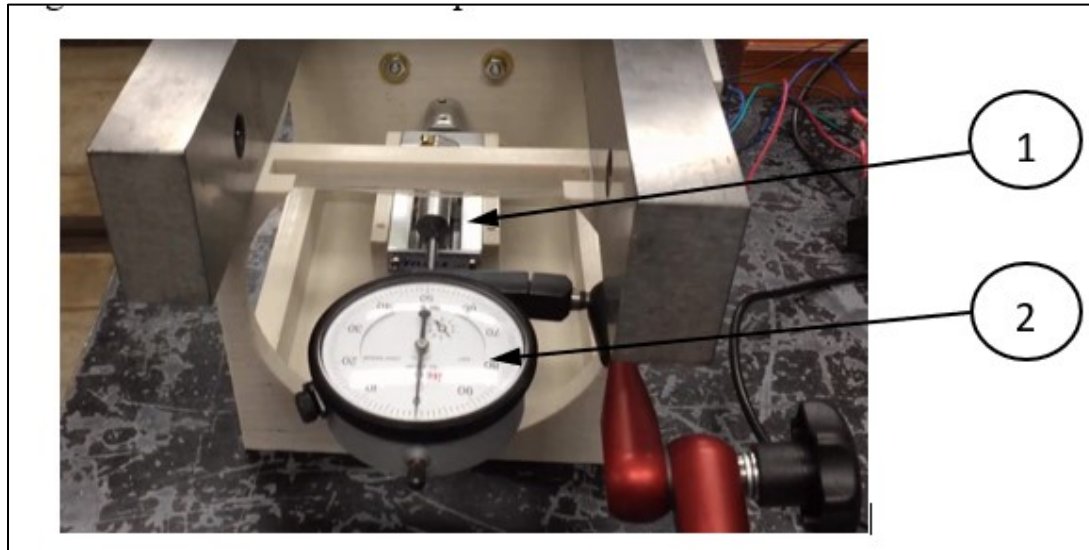


Fig. 19. The position calibration setup

1. Positioning slide

2. Caliper

4.8. Final apparatus system

Fig. 20 shows the final setup for the measurement system. When the top surface is moving, the force and the real time picture are recorded simultaneously. By this setup, the changing of the force is observed with the corresponding changing in shape of the liquid bridge. This setup can be used to conduct experiment for different surface properties, different liquids or different velocities.

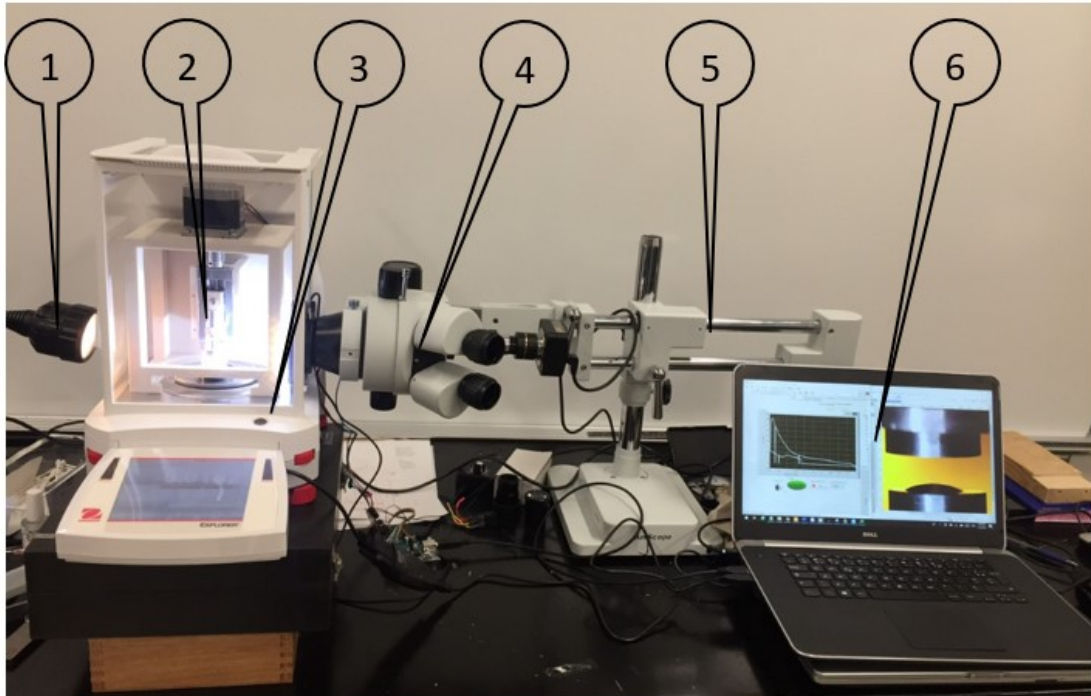


Fig. 20. The experimental system's components

- | | |
|------------------------|-----------------------------------|
| 1. Background lighting | 4. Microscope for image recording |
| 2. Positioning slide | 5. Microscope frame |
| 3. Weight balance | 6. Control and DAQ system |

Fig.21 shows the detail of the final assembly of the positioning slide. The whole frame of the slide is placed inside the weight balance. The weight balance is covered with glass to prevent the external impacts. The sample and the holder are designed to change quickly and exactly. The weight balance has adjustable legs and level indicator to level the balance pan.

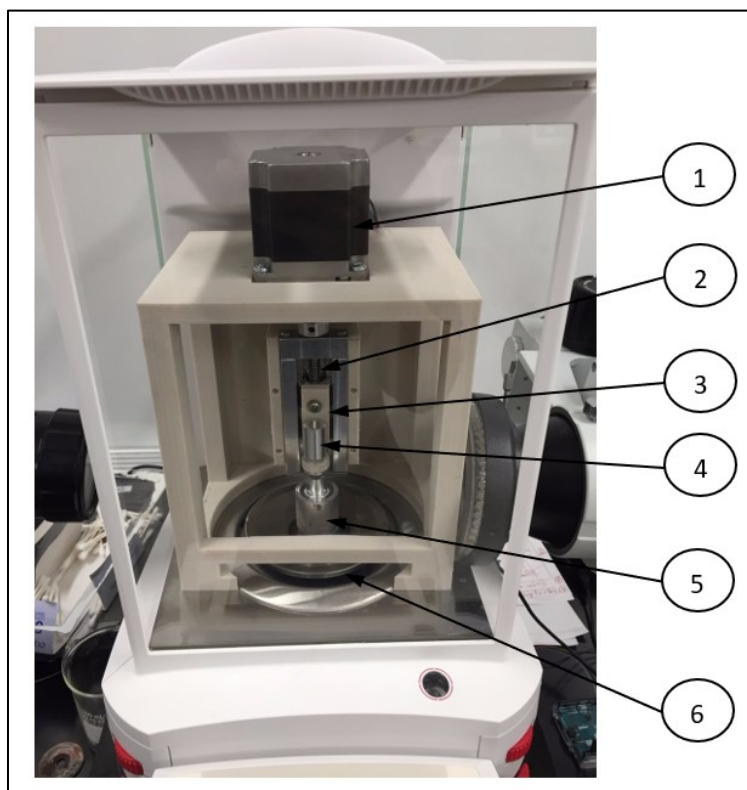


Fig. 21. The final apparatus system

- | | |
|------------------|------------------|
| 1. Step motor | 4. Top sample |
| 2. Lead screw | 5. Bottom sample |
| 3. Sample holder | 6. Weigh balance |

4.9. Image analysis process

The image is obtained from the recorded video, and then the ImageJ software was used to measure the contact angle as shown in Fig. 22. To measure the angle, three points need to be located to create two intersecting lines. The tolerance of the angle measurement depends on camera setup, the height of liquid bridge surface, the resolution of the image and the calibration. The tolerance of angle measurement depends on the way the construction lines

of angle is defined. The position of the construction lines may vary with the subjective observation of people who take the measurement and with the resolution of the image. The tolerance for the angle measurement is $\pm 4^\circ$ from the measurement method. In this study, the relative position of camera and measured contact angle is fixed, but the calibration is not included. Therefore, the contact angle measurement is for reference only, and the tolerance is considered larger than $\pm 4^\circ$. The tolerance used in this study will be $\pm 10^\circ$ to compensate for the lack calibration angle gauge.

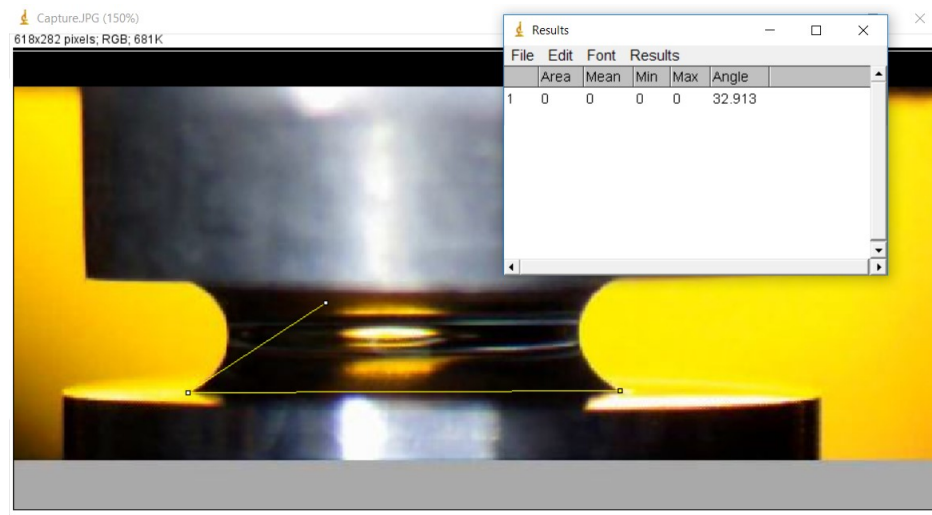


Fig. 22. Angle measurement by ImageJ

To measure length of a line (measured line) on the captured image, a line with known length (gauging line) and its image ratio with the measured line must be defined. The measured line and the gauging line must be in the same surface parallel to image taken surface. For instance, line #1, line #3 shown in Fig. 23 lie in the same surface parallel to the image taken surface and going through the centerline of the concentric cylinders. The

length of line #1 can be calculated by multiplying the image ratio of line #1 and line #3 by the known physical length of line #3. The tolerance of this method is 5-7%.

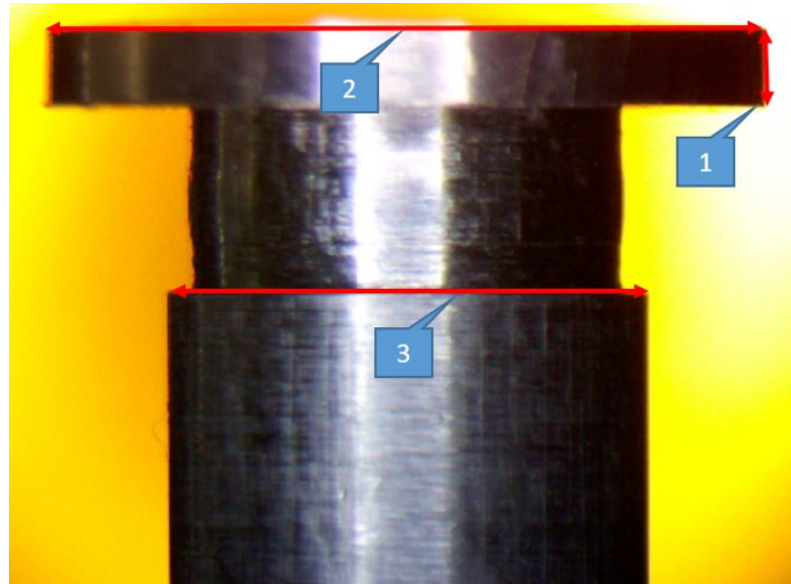


Fig. 23. Distance measurement by ImageJ

5. Experimental Procedure

The liquid tension experimental result depends on many parameters: the distribution of roughness on the surface, the volume of liquid, environment moisture, the tolerance of linear translation system, the maximum contact circle between liquid and solid, the static electric force of two metal surfaces, evaporation process, etc. The experimental procedure must be defined to control those parameters.

To make the roughness value relatively equal on any point in the surface, in the grinding process, we must make sure the ground surface is parallel to the grinding surface and the

ground surface is rotated while grinding. To control volume of the liquid, we use the balance to measure the weight of liquid to define its volume. The process is adding weight more than we desired and then waiting it to evaporate to the desired weight for the fast evaporating liquid. For slowly evaporating liquid, the small amount of liquid is added to the drop until it reaches the weight we want.

To limit the effect of moisture, high percent alcohol is used to dry the surface completely. The tolerance of slide is defined as 0.05 mm in section 4.6. The zero distance needs to be reset after every experiment, and the two surfaces needs to be contacted to eliminate the static electric.

1. Dry the surface with Alcohol 91% – when using the alcohol with lower percent, there is still some very small water residual left on the surface.
2. Insert the sample to the slider holder.
3. Touch two surfaces together reset the distance to zero and discharge the static electricity.
4. Move the upper surface up and add water to the lower surface. The volume of liquid is controlled by the mass of the liquid measured by the weight balance.
5. Use the Microscope with Amscope software to capture images of the bridge and FlashBack Express Recorder to record the whole process.
6. Compress the liquid to the minimum distance – the minimum distance should be chosen so that the contact circle expands completely as discussed above.
7. Immediately pull the bridge to prevent the evaporation.
8. Stop the process, save the video and the data.

6. Experimental Testing and Results

6.1. Process examination

Fig. 24. from step 1 to step 9 show examples of the movement of the base contact circle of a liquid bridge in compression and tension. The rectangle used in the figure is a reference dimension. The steps from 1 to 3 show that the contact base circle is unchanged when the upper surface first touches the liquid drop, and the contact angle increases. When the contact angle reaches to about 90° angle at step 3, the contact base circle expands until the upper surface reaches the minimum presetting distance at step 4. Separating process starts from step 5 and receding of the liquid bridge is observed. The contact angle changes from the advancing angle to the receding contact angle at step 5. At this step, the contact base circle is the largest and a stable contact is formed. Starting from stop 6, the liquid base circle reduced to about its original size, and the contact angle keep unchanged until it breaks from step 5 to step 9.

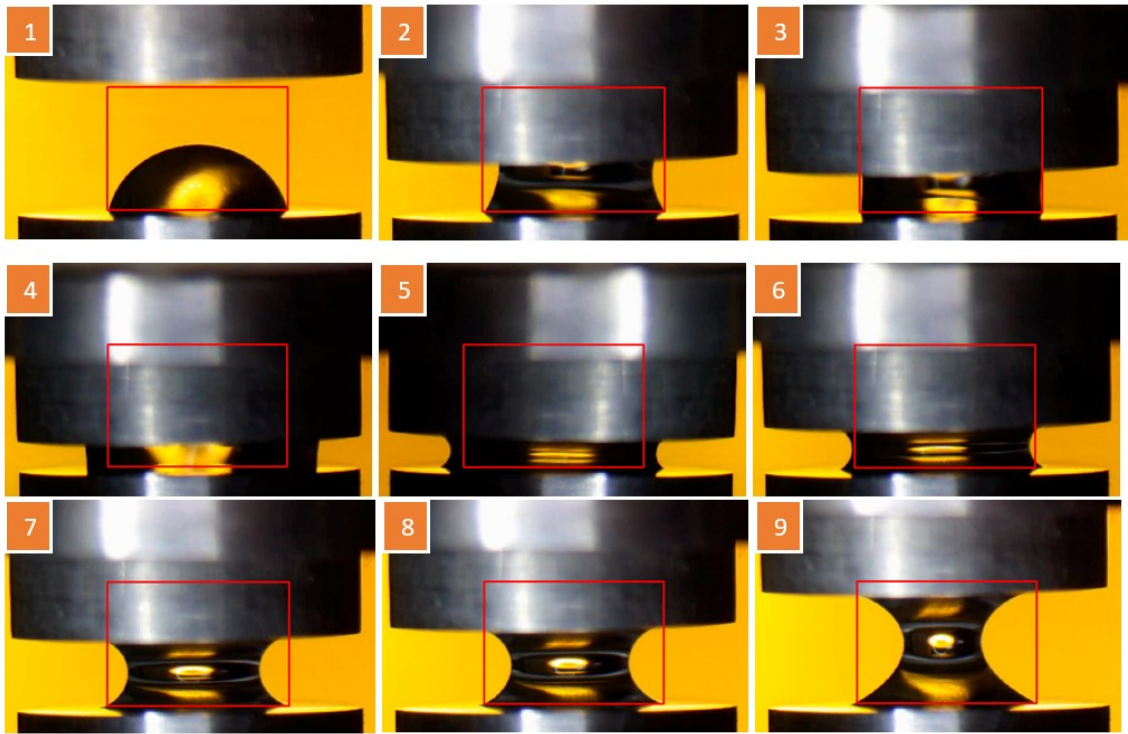


Fig. 24. Contact circle's movement of liquid bridge in compression and tension.

The chart of the corresponding force that describes the whole process (Fig. 22) is shown in Fig. 25. Four sections are divided for convenience of discussion. Section I and II are the approaching process. Section III and IV are the separating process. Section I corresponding to step 1 – 2 shows the process that the upper surface approaches the liquid drop. In section II corresponding to step 2 – 4, the force increases immediately upon the upper surface touches the liquid drop due to the formation of the meniscus. The downward peak in the section shows a missing data point in the data acquisition process. In this section, the force changes due to the change of contact angle, meniscus radius in vertical plane, and neck meniscus radius in horizontal plane. In section III corresponding to step 4 – 5, the force increases rapidly to the maximum value when the contact angle and the meniscus radius

(r_1) reduce. The meniscus force reaches its maximum value when the contact angle changes from the advancing angle to the receding contact angle at step 5. The decrease in contact angle with the same dimension of liquid bridge leads to the decrease of force caused by surface tension – the second term in Eq.1. The decrease in contact angle also leads to the decrease of meniscus radius (r_1) which makes the force caused by the Laplace pressure difference increase – the first term in Eq.1. Therefore, the Laplace pressure is the dominant cause of the formation of the maximum separation force. During the separation process, the force decreases rapidly and slows down later until it breaks.

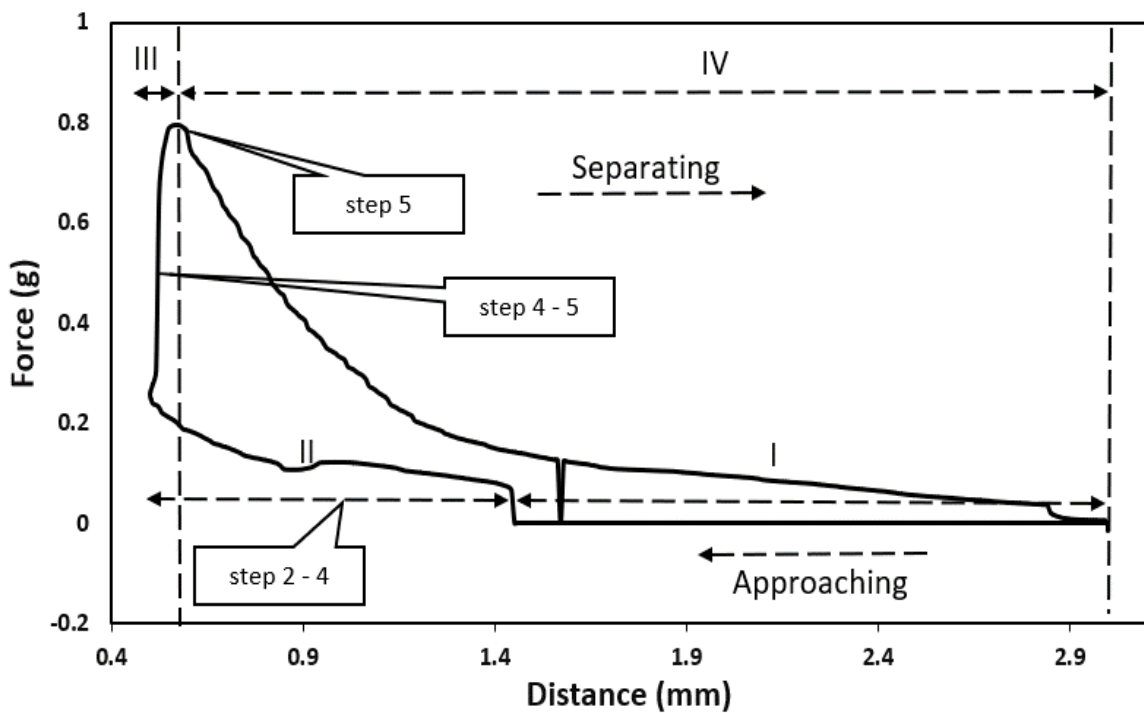


Fig. 25. The force chart for the compression and stretching process.

6.2. Liquid drop analysis

The diameter of contacting circle between liquid drop and surface depends on the way the liquid drop is dispensed on the surface. It depends on the amount of liquid, the dispensing velocity, the height of liquid dispenser. The contacting circle of liquid drop on the surface expands when adding liquid to the drop as shown in Fig.26.

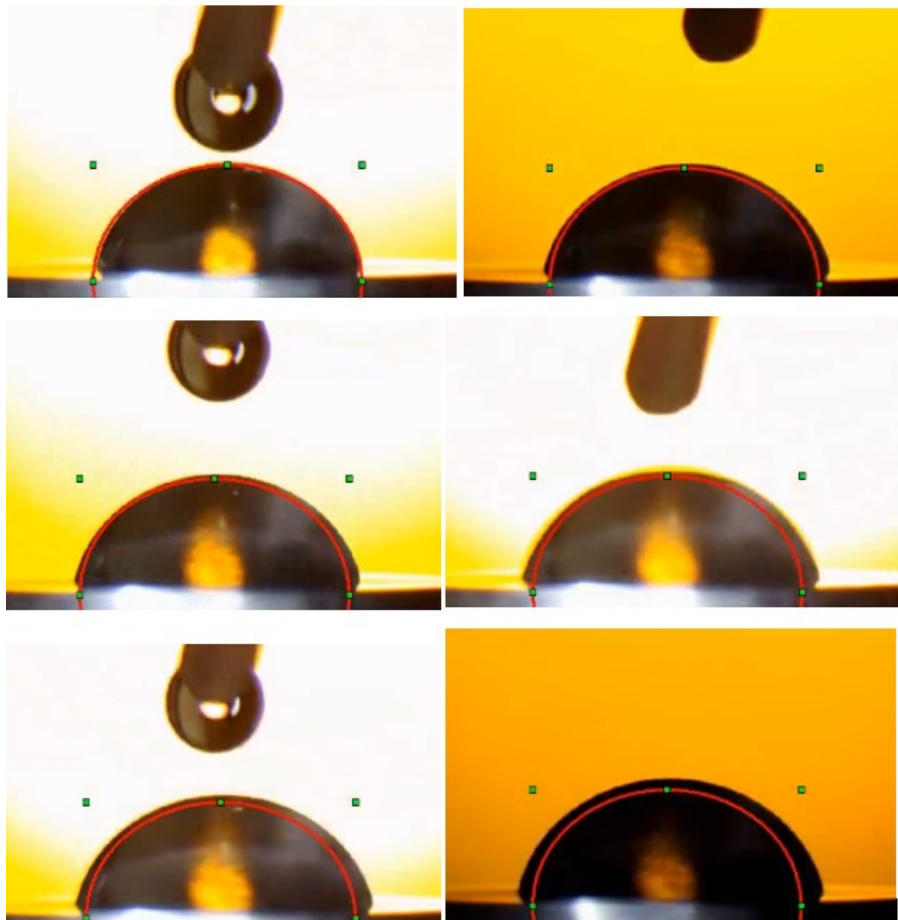


Fig. 26. Contact circle expanding when adding more liquid.

The contacting circle keeps unchanged when evaporation happens as shown in Fig. 27. In the compression process in Fig. 24, the contact circle also keeps unchanged when the contact angle is smaller than 90° and expands when the contact angle reaches about 90° . That means if the minimum distance between the two surfaces is not small enough to expand the contact circle, the contact circle dimension will depend on the way we drop the liquid on the surface. The way we dispense the liquid on the surface is not controlled in this study. The minimum distance between two surfaces must be small enough so that the contacting circle will be expanded completely when the distance between two surfaces is minimum. And by this way, the initial contact circle where the liquid bridge begins to be stretched will be defined by the minimum distance and the volume of liquid only. That means it will not depend on the initial condition in which we drop the liquid on the surface.

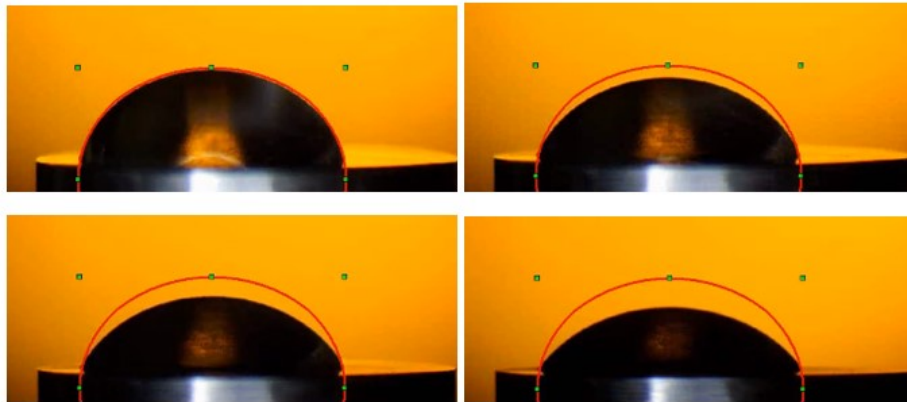


Fig. 27. Contact circle constant in evaporation process

6.3. Force analysis of water in static state

In theory, the meniscus force starts from maximum value and approaches zero when the separation distance increases. In the experiment, however, the force starts from a small value, quickly increases to maximum value and then decreases to zero in the end. If we wait for solid liquid interface to balance – that means waiting the meniscus curve is formed as shown in Fig. 28.

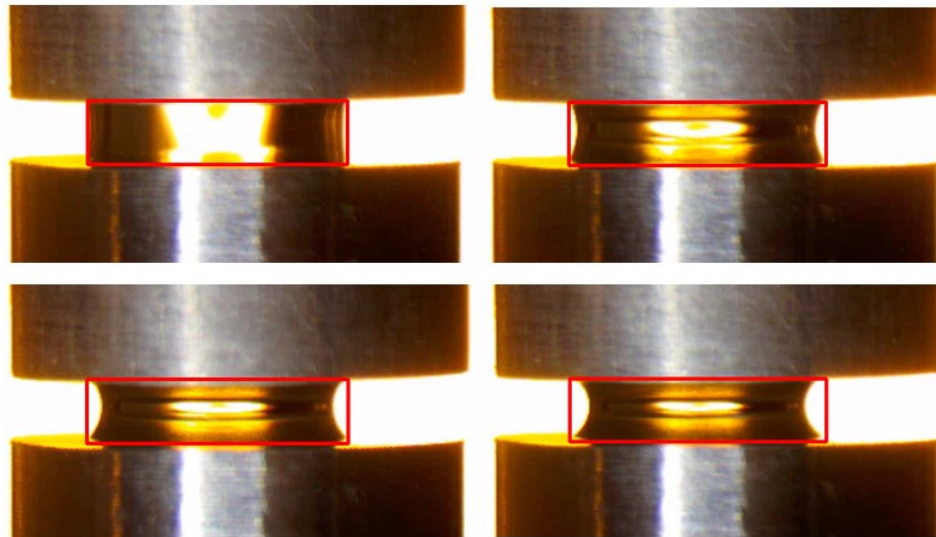


Fig. 28. The evaporation and meniscus formation in water bridge

The force will gradually increase to the maximum value as shown in Fig.29. This figure shows the increasing value of force versus waiting time. The force increasing corresponds to the formation of meniscus curve due to the balancing process and evaporation process. The force reaches its stable value in 4200 (100ms), 420 seconds or 7 minutes.

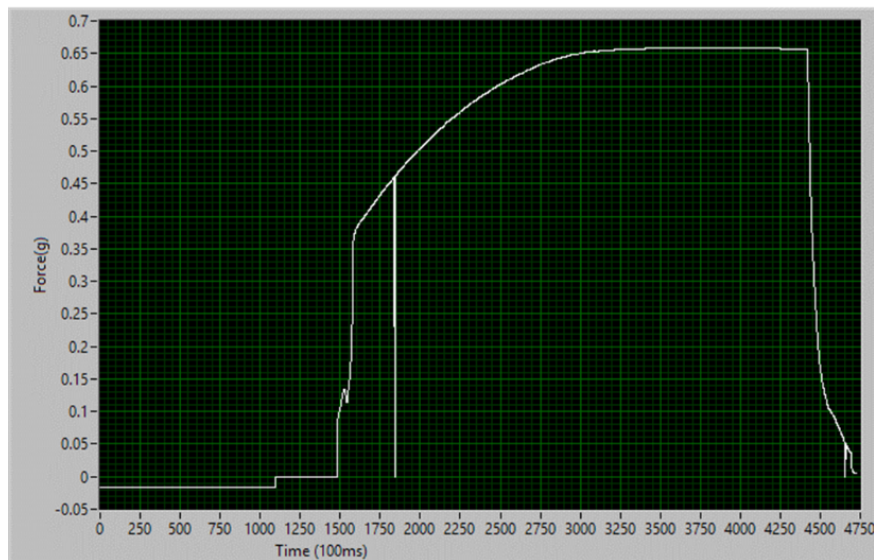


Fig. 29. Force vs time graph when evaporation occurs in water bridge.

If pull the bridge at the time the meniscus force reaches the maximum value, the force will immediately start to reduce from the maximum value as described in theory and shown in Fig. 30. However, when waiting the force increases, the liquid also evaporates, and this process will change the initial volume of the liquid bridge. After the evaporation happens, the weight or the volume of the liquid can not be defined by the weight balance due to the effect of the meniscus force.

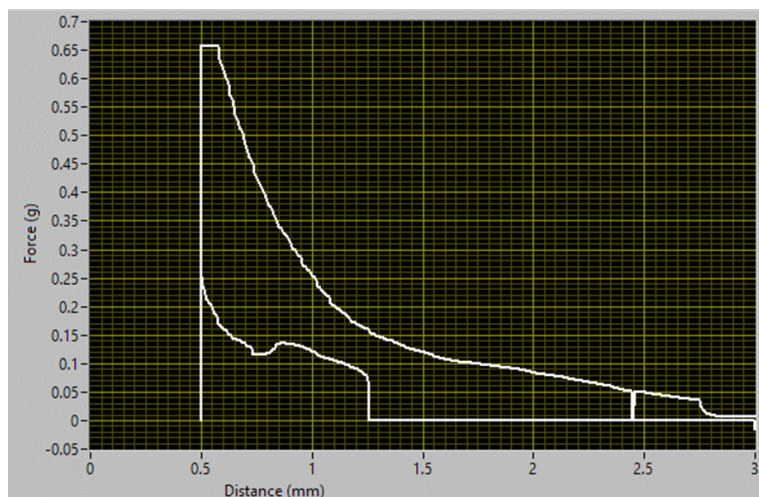


Fig. 30. The force vs distance graph after waiting for the meniscus to form in water

To evaluate the evaporation rate of liquid (water in this study), the free drop of water is put on the weight balance, and the weigh drops from 0.02g to 0.0145g in 850 s or 14 min, i.e. the weight of drop decreases 27.5% in 14 minutes or 13.75% in 7 minutes as shown in Fig.31. Therefore, the waiting time for the meniscus formation can not be added to the experimental process.

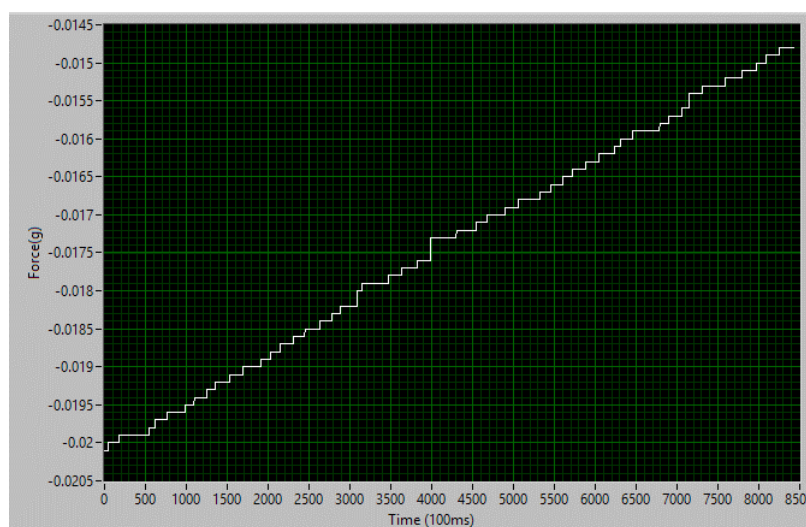


Fig. 31. The evaporation of free standing drop on the surface.

6.4. Force analysis of glycerol in static state

For the liquid with slower evaporation rate considered as nonvolatile liquid (glycerol in this study), the glycerol drop is compressed and kept at the minimum distance to wait for the meniscus force to balance as the process for water shown in Fig.28. The meniscus force increases rapidly to certain value about 0.35 g and stays there until the top surface moves as shown in Fig. 32. When the top surface moves up at 4500 on Time - axis, the force still increases to the maximum value before going down.

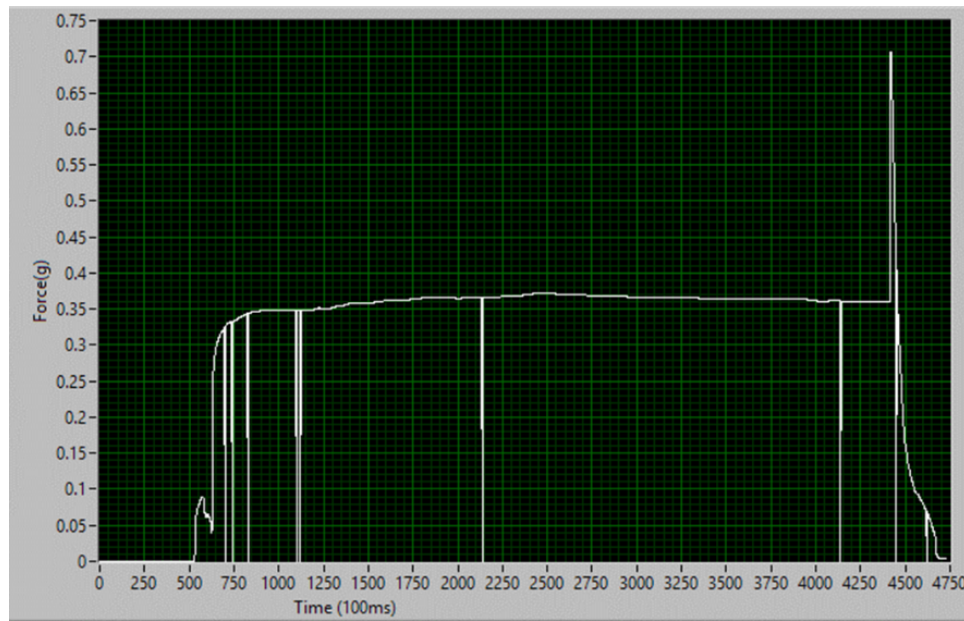


Fig. 32. Force vs time graph when meniscus formation occurs in glycerol bridge

In the graph of force versus distance, if we wait for the meniscus curve to form at the minimum distance 0.5mm as shown in Fig. 33, the force will increase to the certain value 0.35g similar to Fig.32. When the top surface is pulled up, the force still increases to its

maximum before decreasing. Fig. 33 shows the meniscus force after the time waiting for meniscus balance with respect to distance.

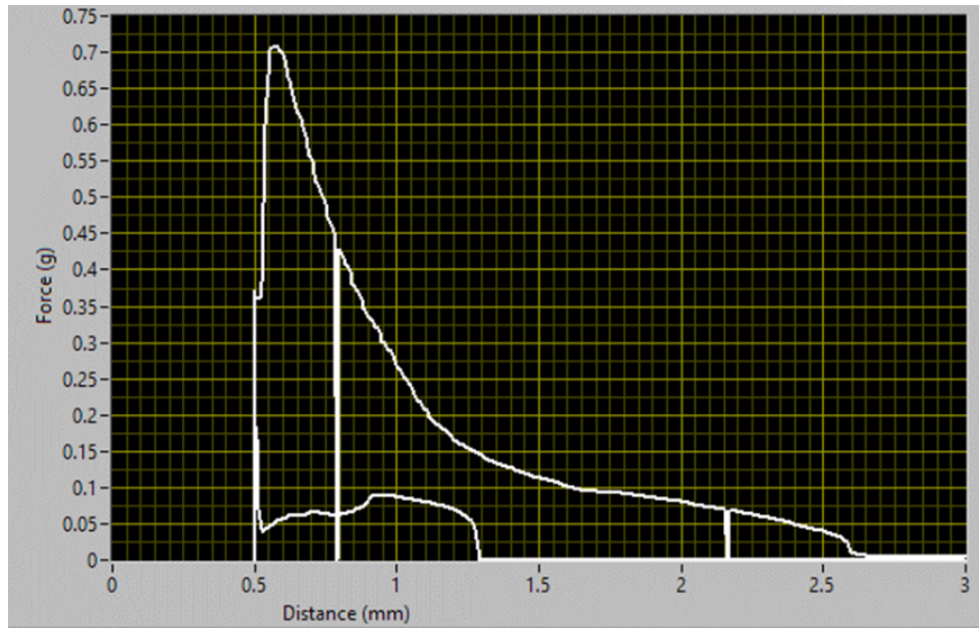


Fig. 33. The force vs distance graph after waiting for the meniscus to form in glycerol.

When the meniscus bridge stays unchanged and stable shown in Fig. 32, the curvature and the contact angle of meniscus curve in glycerol is called the stable curvature and contact angle as shown in Fig. 34 a. When the liquid bridge is stretched, the curvature and the contact angle of the meniscus curve is called the receding curve and receding contact angle as shown in Fig. 34 b. Considering red lines shown in Fig. 34 a & b as the reference lines, the stable curvature is smaller than the receding curvature (or the curve radius is larger than that in the receding situation), and the stable contact angle is larger than the receding contact angle. When the glycerol bridge changes from its stable state to its stretched state, the transition from the stable contact angle to the receding contact angle results in the increase in separation force.

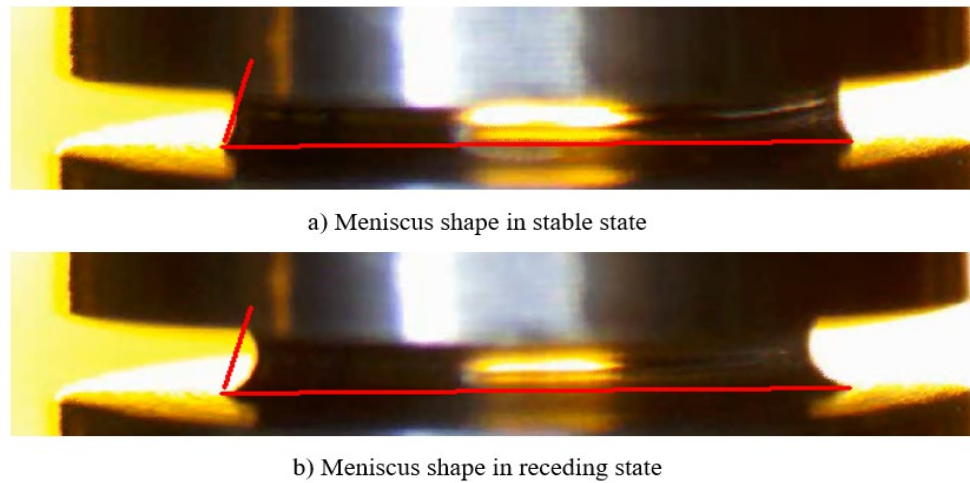


Fig. 34. The meniscus shape of glycerol in different states.

In liquid with higher evaporation rate - water bridge, the evaporation makes the stable curvature of the meniscus bridge larger and closer to its receding curvature as shown in Fig. 35. The stable contact angle is closer to the receding contact angle. The transition between stable and receding states is quite small when the bridge is stretched. This explains why the increasing of separation force can not be seen when the water bridge is stretched as shown in Fig. 30. From the observation of water and glycerol, the evaporation has a certain impact on the forming process of meniscus bridge. The evaporation will change the geometric parameters such as the contact angle, the vertical radius or the horizontal radius of liquid bridge, and the change of geometric parameters will lead to the change of meniscus force in static state. To create a consistent process, the waiting time will be not added to the process, and the liquid bridge is stretched immediately after being compressed to the minimum distance.

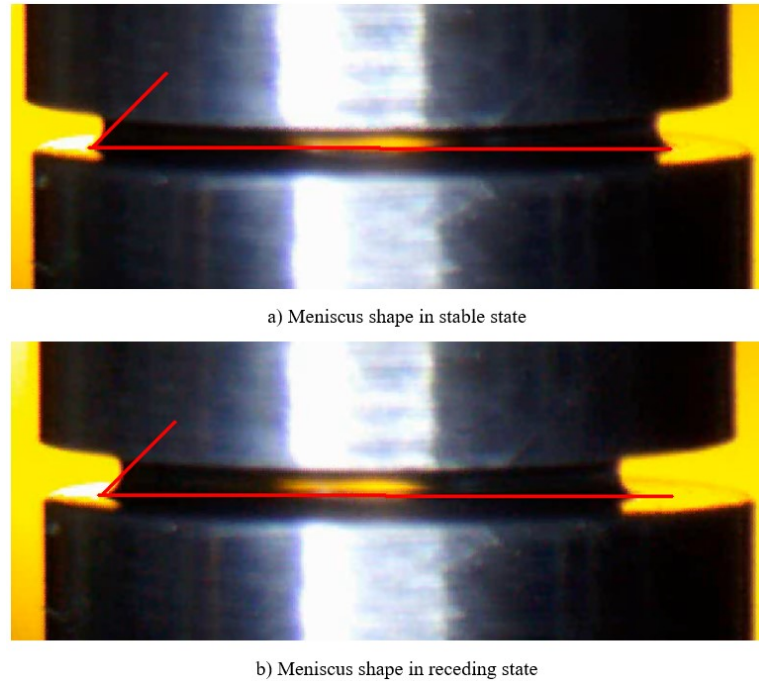


Fig. 35. The meniscus shape of water in different states.

7. Comparison Studies of Design Parameters

The experiments are conducted with two liquids: water and glycerol (glycerin). They have different density and surface tension. The volume of each drop is controlled the same in every experiment by controlling their mass. They are tested under the same room condition and initial setup. The experimental parameters of water and glycerol are listed in Table. 3. The water and glycerol are chosen because of their difference in evaporation rate. The evaporation rate is indicated by the vapor pressure of liquid. The higher the vapor liquid is, the higher the evaporation rate is. The vapor pressure of water at the ambient temperature is 25.8 mmHg, and that of glycerol is below 0.001 mmHg [23]. Glycerol is consider a nonvolatile liquid.

Table 3. The experiment parameters of water and glycerol.

Experimental parameters for water	Experimental parameters for glycerol
Density: 1000 kg/m ³	Density: 1261 kg/m ³
Surface tension: 7.2 x 10 ⁻² N/m	Surface tension: 6.3 x 10 ⁻² N/m
Controlled mass: 1.5 x 10 ⁻⁵ kg	Controlled mass: 1.9 x 10 ⁻⁵ kg
Controlled volume: 1.5 x 10 ⁻⁸ m ³	Controlled volume: 1.5 x 10 ⁻⁸ m ³
Temperature: 25°C	Temperature: 25°C
Humidity: 50%	Humidity: 50%
Vapor pressure: 25.8 mmHg	Vapor pressure: below 0.001 mmHg
Surface material: Aluminum	Surface material: Aluminum
Minimum distance: 0.5 mm	Minimum distance: 0.5 mm
Operation velocity: 0.079 mm/s	Operation velocity: 0.079 mm/s

7.1. Water and design parameters

7.1.1. Effect of surface roughness preparations

Experiment with water drop is conducted with aluminum surfaces ground by sandpapers with different GRIT such as GRIT #240, GRIT #400, and GRIT #600. Following the experimental steps in Section 5 with the initial parameters listed in Table. 3, the separation force with respect to displacement for each prepared surface and each liquid is recorded to

study. The experimental data for the surface prepared by #240 sandpaper is presented in Fig. 36. The trend of force curve follows the description of general force curve presented in Section 6.1. The graph includes Approaching process, Separating process, the Compression section II, the Stretching section III and IV, and therein the section III is the transition from the advancing angle to receding angle.

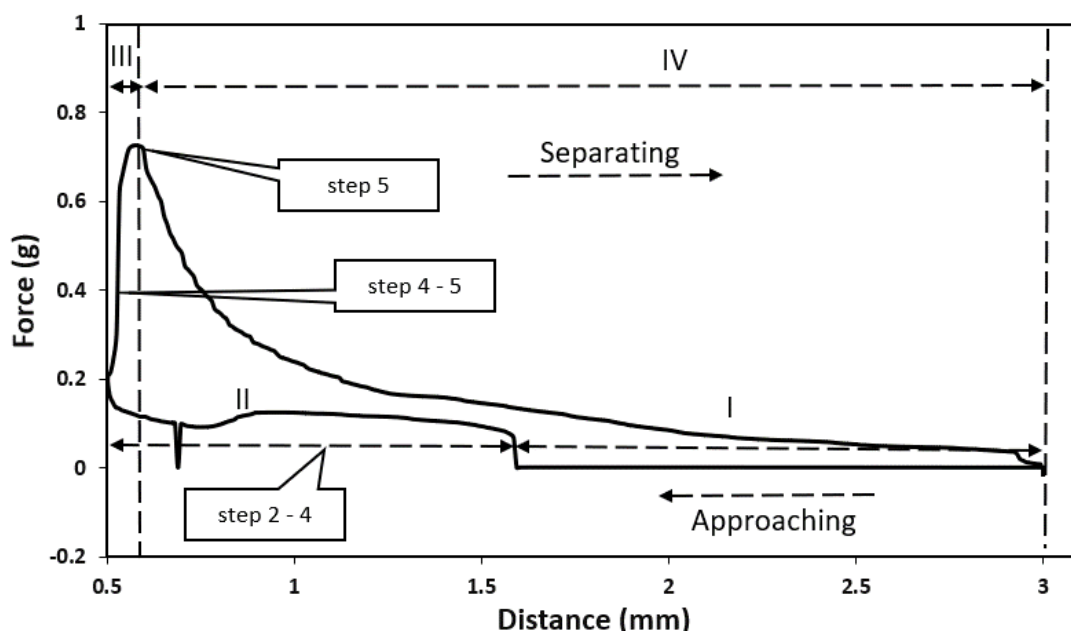


Fig. 36. The force displacement curve of water bridge with surface ground by #240 sandpaper.

The similar force displacement curves are observed for surface with different sandpaper preparations and different liquids. The force curve for each case then is compared with the theoretical separating force curve created with the same experimental parameters as shown in Fig. 37 for the water bridge with surface ground by #240 sandpaper case. The angle used for theoretical calculation is the receding angle measured when the liquid bridge is stretched to a certain distance. The maximum force in the experimental data is highlighted

on the graph. The experimental force curve follows the trend of theory created force curve. There is a deviation around the maximum value of the separation force due to the deviation of minimum distance between two surfaces. The comparison is conducted only for the stretching section because change of contact angle in the compression section is more complicated and depends on the wetting status of the surface.

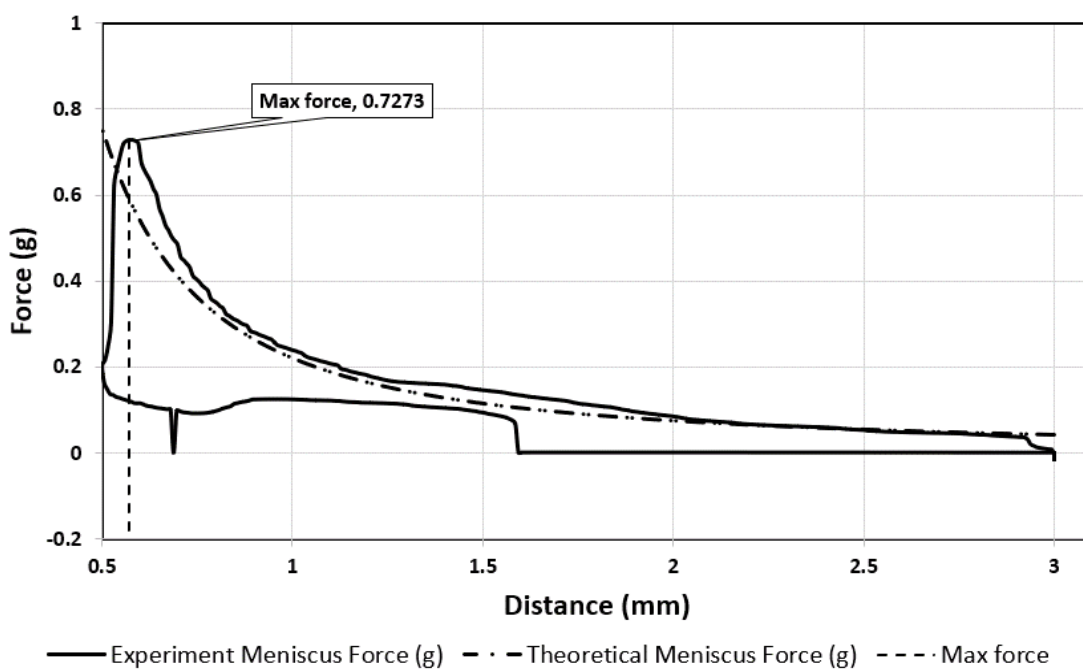


Fig. 37. The force curve comparison of water bridge with surface ground by #240 sandpaper.

The cyclic run is conducted to test the repeatability of the system. The experiment includes 5 complete cycles of compression and stretching from the height 2 mm to prevent the break of liquid bridge as shown in Fig. 38. Except for the first compression curve, the force curve repeated in every cycle. This repeated cycle presents the stability of the system. The speed of the slider, the distance and the force measurement are

controlled accurately. The exception at the first compression curve is explained by the wetting state of the surface. The wetting state of the surface changes the advancing contact angle.

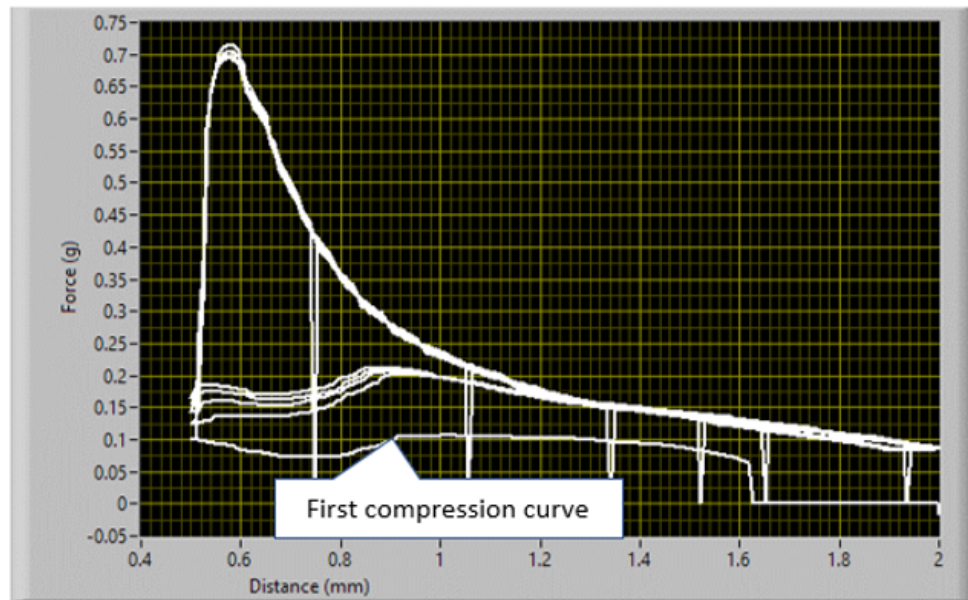


Fig. 38. Cyclic run experiment of water on the #240 ground surface.

The similar process is applied for surfaces with different roughness preparations. The receding angle and the maximum force for each experiment are recorded in Table. 4. The observations for the other experiments are identical to these in the experiment of water bridge with surface ground by #240 sandpaper. The experimental force curves are almost aligned with the theory created force curve. There is a deviation around the maximum value of the separation force due to the deviation of minimum distance between two surfaces.

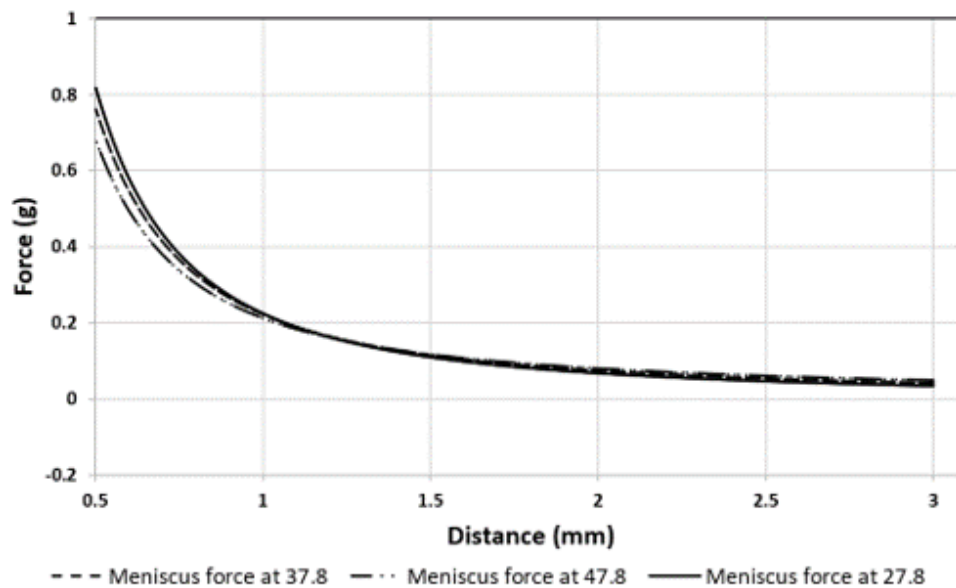
Table 4. The experiment result of water drop with different surface preparation

GRIT #240	GRIT #400	GRIT #600
Contact angle = 37.5	Contact angle = 38.7	Contact angle = 37.3
Maximum force = 0.73 g	Maximum force = 0.74 g	Maximum force = 0.74 g
Force curve		

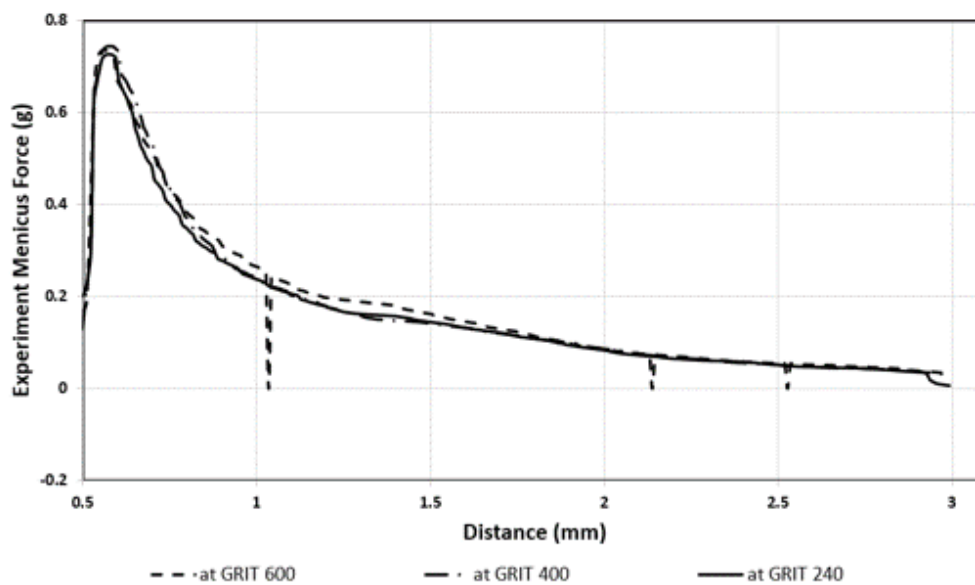
Table. 4. The experiment result of water drop with different surface preparation (cont.)

Repeated run		
Theory comparison		

In Table. 4, the variation of contact angle for different roughness surfaces is not significant. The average contact angle is 37.8° . As presented in Section 4.9, the tolerance the contact angle measurement is given $\pm 10^\circ$. The contact angle for different roughness is assumed to range from 27.8° to 47.8° . The contact angles are used to create the theoretical graph will be 27.8° , 37.8° , and 47.8° . Fig. 39a presents the theoretical graphs of meniscus force with the contact angles above and the experimental parameters are listed in Table. 3 for water. In theory, if the change of the contact angle is $\pm 26\%$ (47.8° , 37.8° , and 27.8°), the change of the maximum meniscus force is -10% to $+7\%$ (0.68g , 0.76g , and 0.82g). Fig.39b is the meniscus force with different roughness for water bridge. The deviation of maximum separation force is not observed in the experiments with different roughness.



a)



b)

Fig. 39. The theoretical and experimental graph for different surface roughness for water:

a) The theoretical graph with different contact angles, b) The experimental graph with different surface preparation.

7.1.2. Effect of volume/mass

In theory, if the change of the volume or mass of the water is $\pm 20\%$ (0.012 g, 0.015g, and 0.018g), the change of the maximum meniscus force is considerable $\pm 19\%$ (0.56g, 0.69g, and 0.82g) as shown in Fig. 40. Comparing with the change of force with contact angle deviation in section 7.1.1., the change of force caused by volume or mass deviation is more significant than that caused by the contact angle deviation. The change of volume could affect the force measurement. In this study, however, the tolerance volume or mass of liquid is controlled under $\pm 5\%$ by the weight balance with the readability 0.0001g.

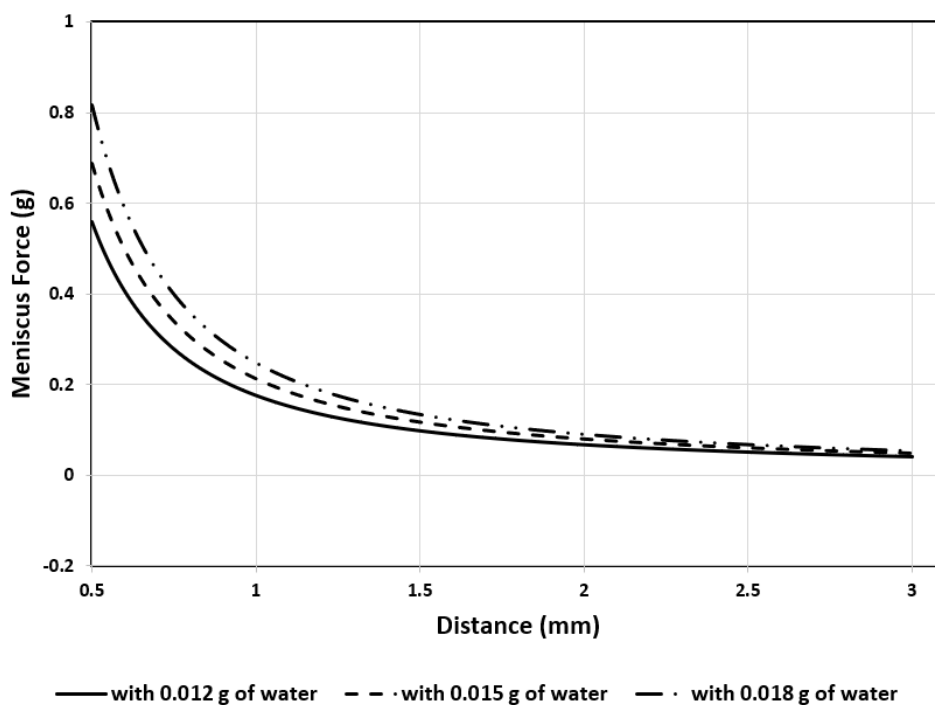


Fig. 40. Theoretical results for different volume or mass liquids with the same initial conditions.

7.1.3. Effect of minimum distance

In theory, with different minimum distances, the meniscus forces curve is the same but the maximum forces are different as shown in Fig. 41. If the change of the minimum distance is $\pm 10\%$ (0.45 mm, 0.5 mm, and 0.55 mm), the change of the maximum meniscus force is quite large -15% to 21% (0.58g, 0.69g, and 0.83g). Comparing with the change of force with contact angle deviation in section 7.1.1, the change of force caused by minimum distance deviation is more significant than that caused by the contact angle deviation. The change of minimum distance really affects the force measurement. The tolerance of sliding position 0.05 mm as stated in section 4.7 and the deviation in height of ground surface affect the minimum distance and make the experiment result uncertain.

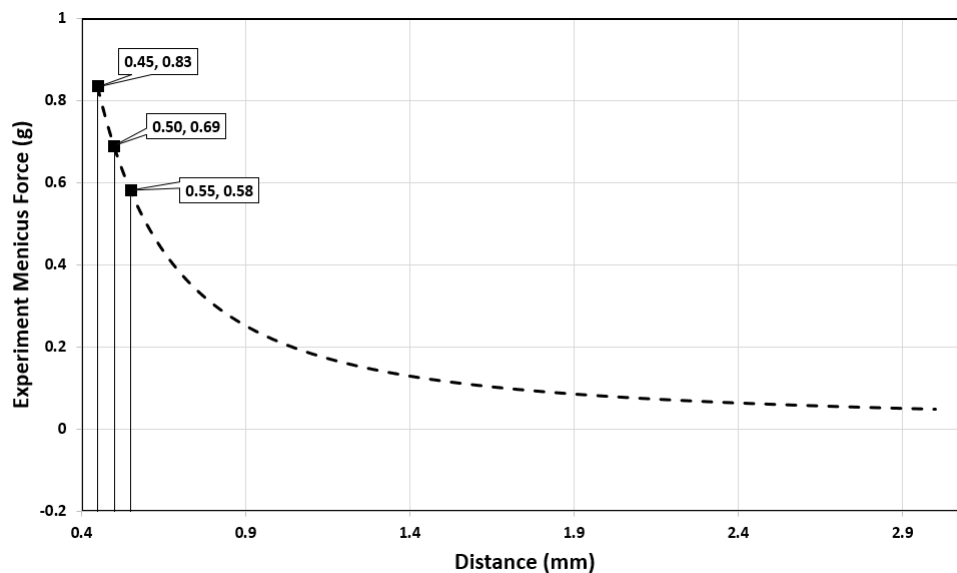


Fig. 41. The theory graph for different minimum distances with the same initial conditions for water.

7.2. Glycerol and design parameters

7.2.1. Effect of surface roughness preparations

Experiment with glycerol drop is conducted with aluminum surfaces ground by sandpapers with different GRIT such as GRIT #240, GRIT #400, and GRIT #600. Following the experiment steps in Section 5 with the initial parameters listed in Table. 3, the separation force with respect to displacement for each prepared surface and each liquid is recorded to study. The experiment data for the surface prepared by #240 sandpaper is presented in Fig.42. The trend of force curve follows the description of general force curve presented in Section 6.1. The graph includes Approaching process, Separating process, the Compression section II, the Stretching section III and IV, and therein the section III is the transition from the advancing angle to receding angle.

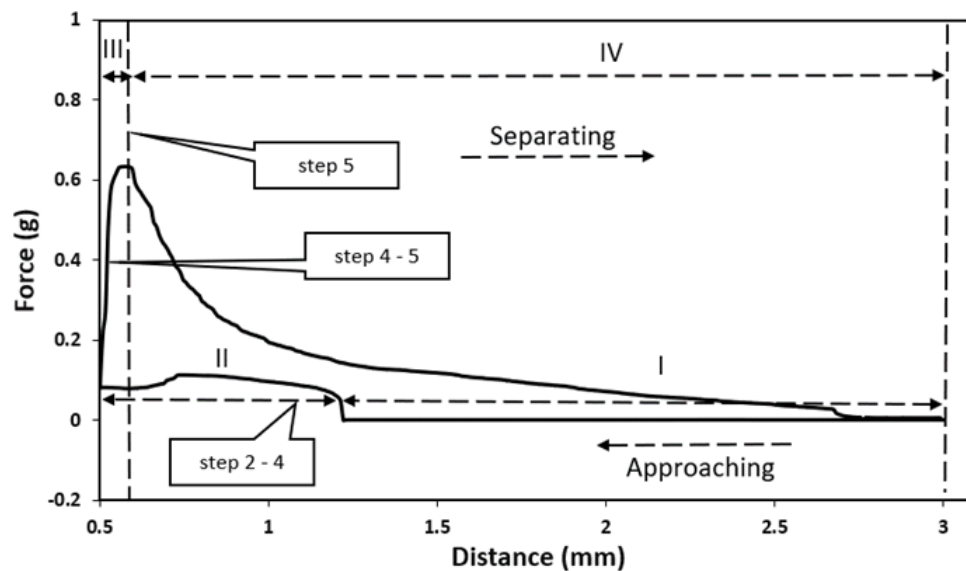


Fig. 42. The force displacement curve of glycerol bridge with surface ground by #240 sandpaper.

The similar force displacement curves are observed for surface with different sandpaper preparations. The force curve for each case then is compared with the theory separating force curve created with the same experiment parameters as shown in Fig. 43 for the glycerol bridge with surface ground by #240 sandpaper case. The angle used for theory calculation is the receding angle measured when the liquid bridge is stretched to a certain distance. The maximum force in the experiment data is highlighted on the graph. The experiment force curve follows the theory created force curve. There is a deviation around the maximum value of the separation force due to the deviation of minimum distance between two surfaces. The comparison is conducted only for the stretching section because change of contact angle in the compression section is more complicated and depends on the wetting status of the surface.

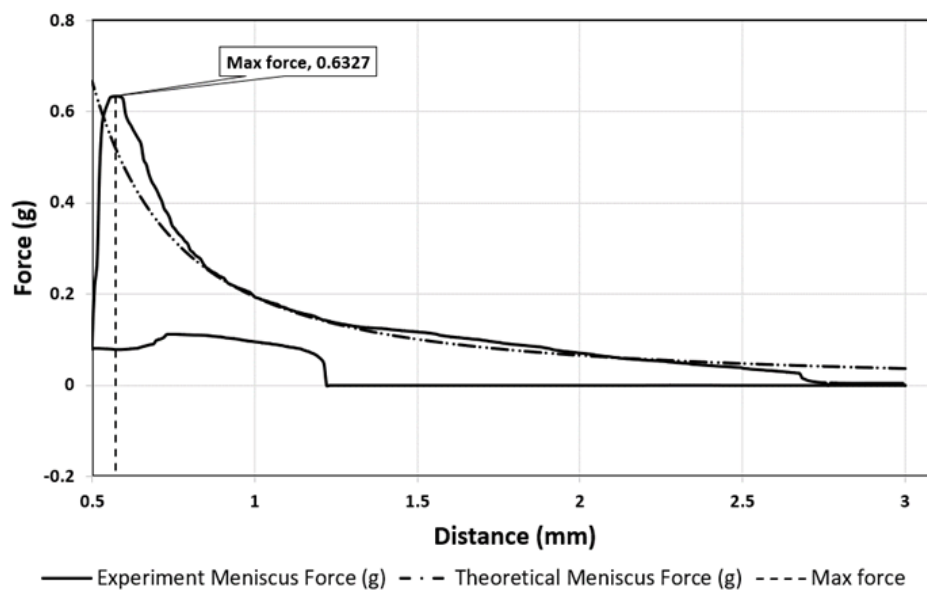


Fig. 43. The force curve comparison of glycerol bridge with surface ground by #240 sandpaper.

The cyclic run is conducted to test the repeatability of the system. The experiment includes 5 complete cycles of compression and stretching from the height 2 mm to prevent the break of liquid bridge as shown in Fig. 44. Except for the first compression curve, the force curve repeated in every cycle. This repeated cycle presents the stability of the system. The speed of the slider, the distance and the force measurement are controlled accurately. The exception at the first compression curve is explained by the wetting state of the surface. The wetting state of the surface changes the advancing contact angle.

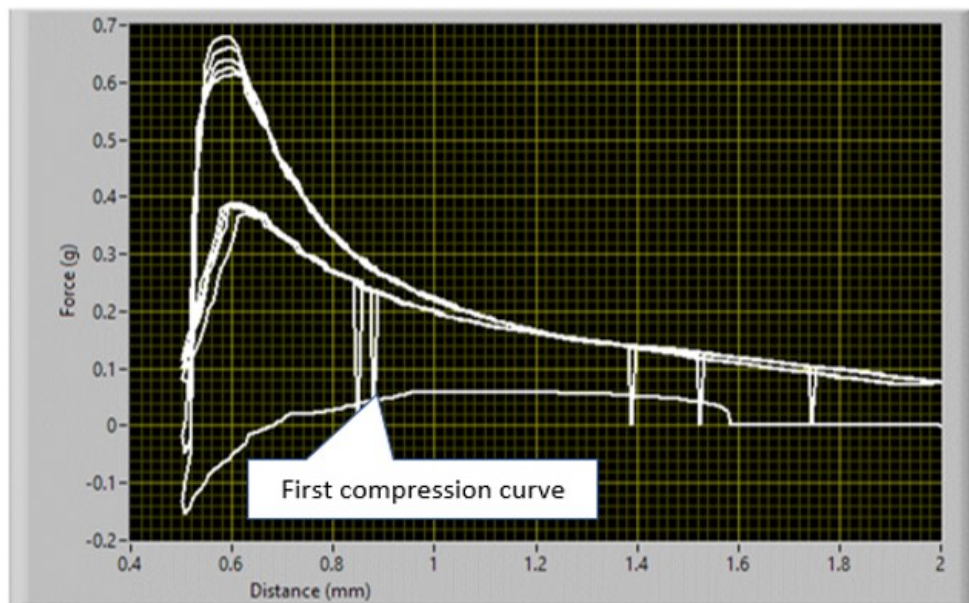


Fig. 44. Cyclic run experiment of glycerol on the #240 ground surface.

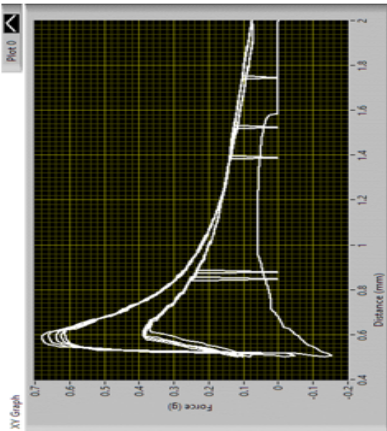
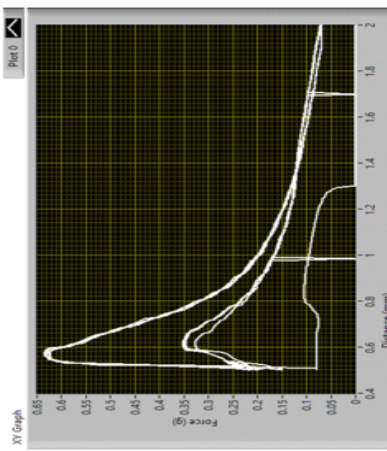
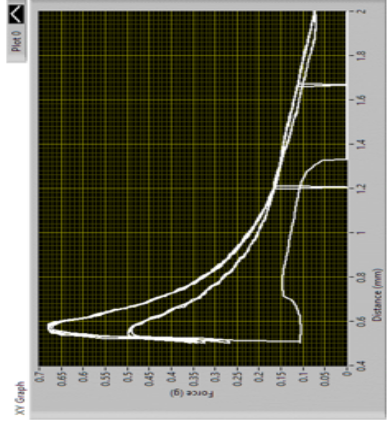
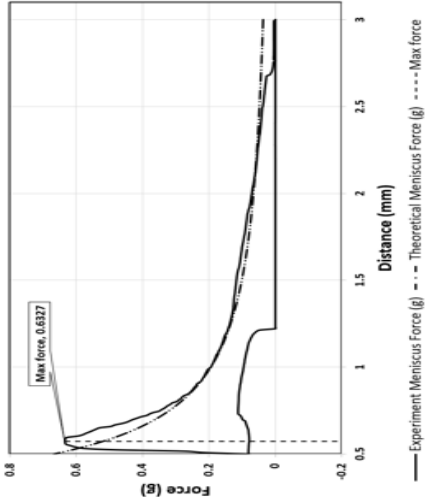
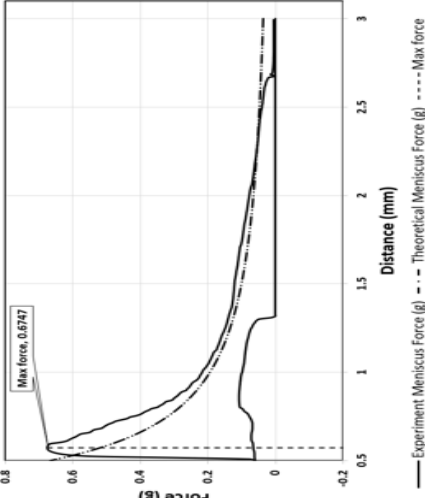
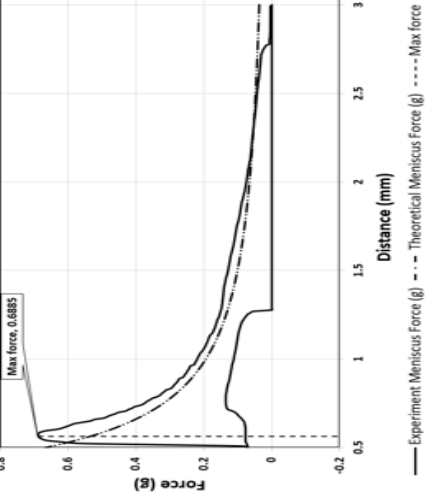
The similar process is applied for surfaces with different roughness preparations. The receding angle and the maximum force for each experiment are recorded in Table. 5. The observations for the other experiments are identical to these in the experiment of glycerol bridge with surface ground by #240 sandpaper. The experiment force curves are almost

aligned with the theory created force curve. There is a deviation around the maximum value of the separation force due to the deviation of minimum distance between two surfaces.

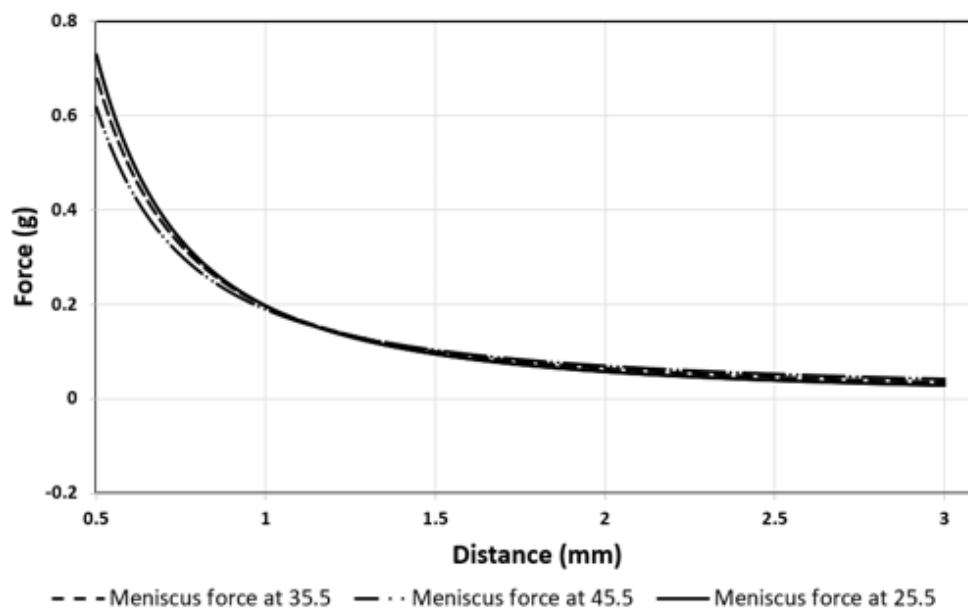
Table. 5. The experiment result of glycerol drop with different surface preparation

GRIT #240	GRIT #400	GRIT #600
Contact angle = 35.7	Contact angle = 36	Contact angle = 34.7
Maximum force = 0.63 g	Maximum force = 0.67 g	Maximum force = 0.69 g
Force curve		

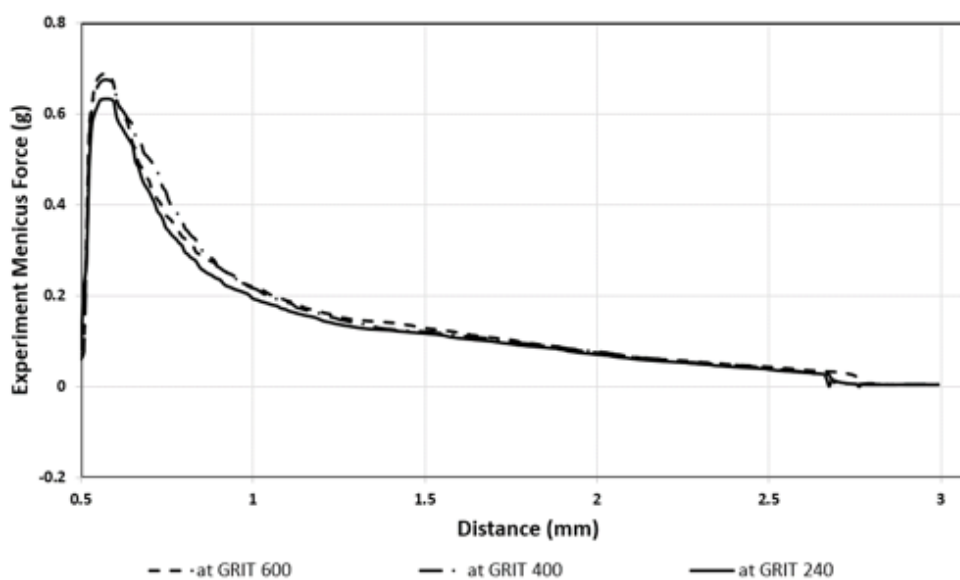
Table. 5. The experiment result of glycerol drop with different surface preparation (cont.)

GRIT #240	GRIT #400	GRIT #600
Repeated run		
		
Theory comparison		
		

The similar methodology is conducted for glycerol to create the theoretical and experimental graph for different surface roughness. The contact angles are used to create the theoretical graph will be 25.5° , 35.5° , and 45.5° . Fig. 45. shows the theoretical and experimental graph for different surface roughness for glycerol. Fig. 45a presents the theoretical graphs of meniscus force with the contact angles above and the experimental parameters are listed in Table. 3 for glycerol. In theory, if the change of the contact angle is $\pm 28\%$ (45.5° , 35.5° , and 25.5°), the change of the maximum meniscus force is -10% to $+7\%$ (0.62g, 0.68g, and 0.73g). Fig.45b is the meniscus force with different roughness for glycerol bridge. The deviation of maximum separation force is not observed in the experiments with different roughness



a)



b)

Fig. 45. The theoretical and experimental graph for different surface roughness for glycerol: a) The theoretical graph with different contact angles, b) The experimental graph with different surface preparation.

According to Wenzel [24], the contact angle is smaller on a rougher surface of the same material for hydrophilic contacts. The deviation of contact angle for different roughness could not be observed in this study due to the tolerance of angle measurement. In Fig. 38a the contact angle is assumed to vary $\pm 10^\circ$, and the maximum meniscus force decreases when the contact angle is larger. In Fig. 38b, the experimental maximum forces for different roughness are aligned with the average maximum force in theory. The experimental maximum forces do not show the variation with the different roughness. The similar observation is presented in the experiments of glycerol with different surface roughness.

7.2.2. Effect of volume/mass

In theory, if the change of the volume or mass of the glycerol is $\pm 20\%$ (0.0152 g, 0.019g, and 0.0228g), the change of the maximum meniscus force is considerable $\pm 19\%$ (0.55g, 0.69g, and 0.82g) as shown in Fig. 46. Comparing with the change of force with contact angle deviation in section 7.2.1, the change of force caused by volume or mass deviation is more significant than that caused by the contact angle deviation. The change of volume could affect the force measurement. In this study, however, the tolerance volume or mass of liquid is controlled under $\pm 5\%$ by the weight balance with the readability 0.0001g.

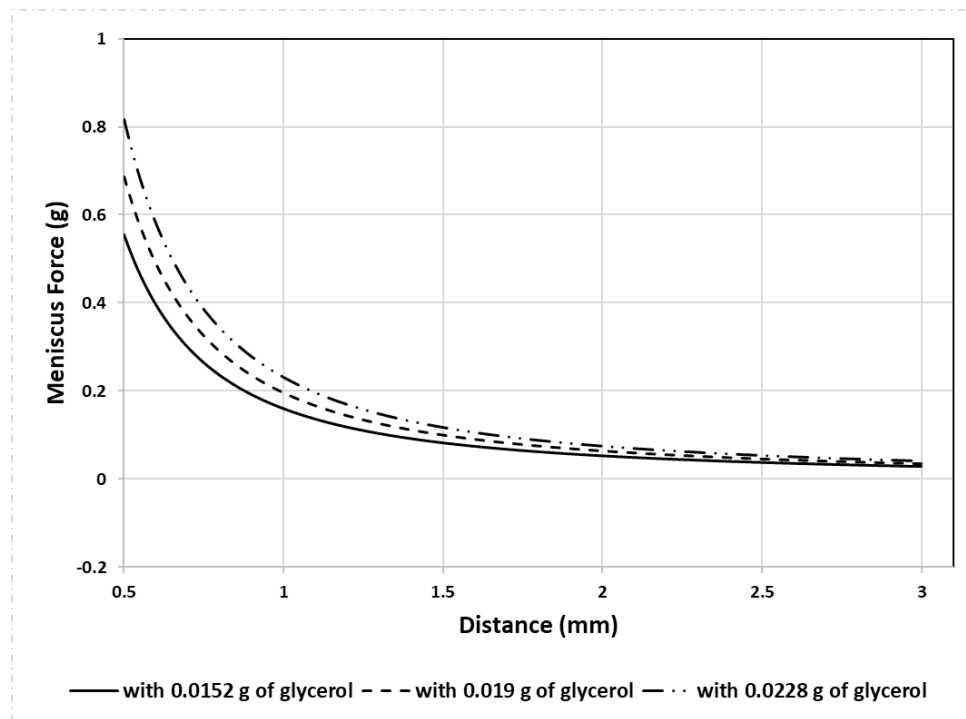


Fig. 46. Theoretical results for different volume or mass liquids with the same initial conditions for glycerol

7.2.3. Effect of minimum distance

In theory, with different minimum distances, the meniscus forces curve is the same but the maximum forces are different as shown in Fig. 47. If the change of the minimum distance is $\pm 10\%$ (0.45 mm, 0.5 mm, and 0.55 mm), the change of the maximum meniscus force is quite large -16% to 22% (0.57g, 0.69g, and 0.84g). Comparing with the change of force with contact angle deviation in section 7.2.1, the change of force caused by minimum distance deviation is more significant than that caused by the contact angle deviation. The change of minimum distance really affects the force measurement. The tolerance of sliding

position 0.05 mm as stated in section 4.7 and the deviation in height of ground surface affect the minimum distance and make the experimental result uncertain.

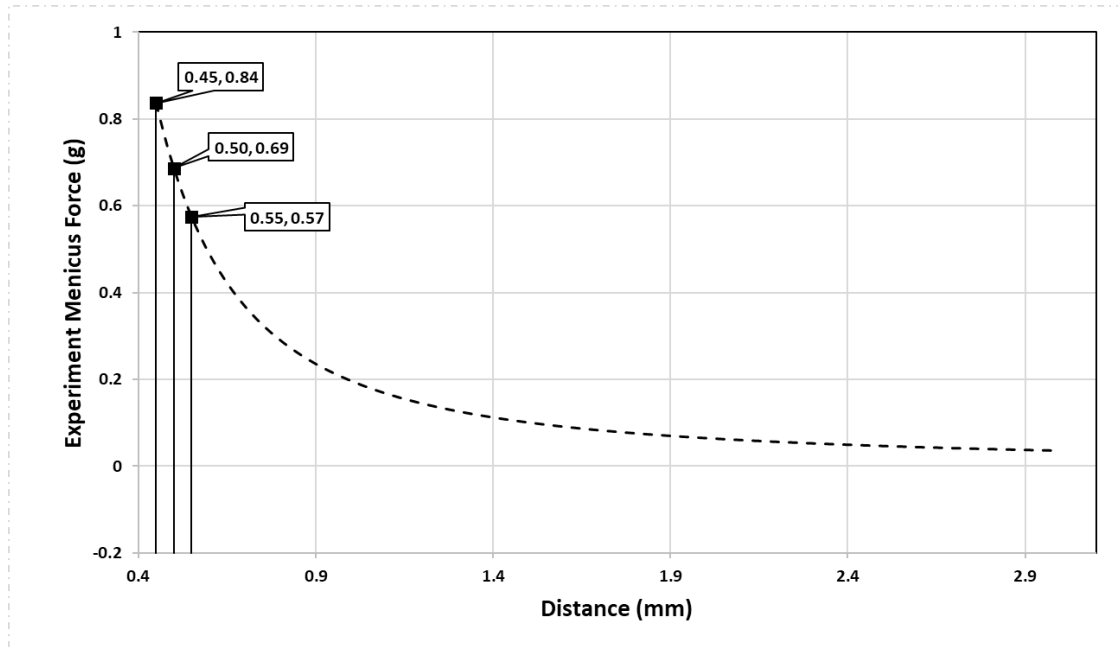
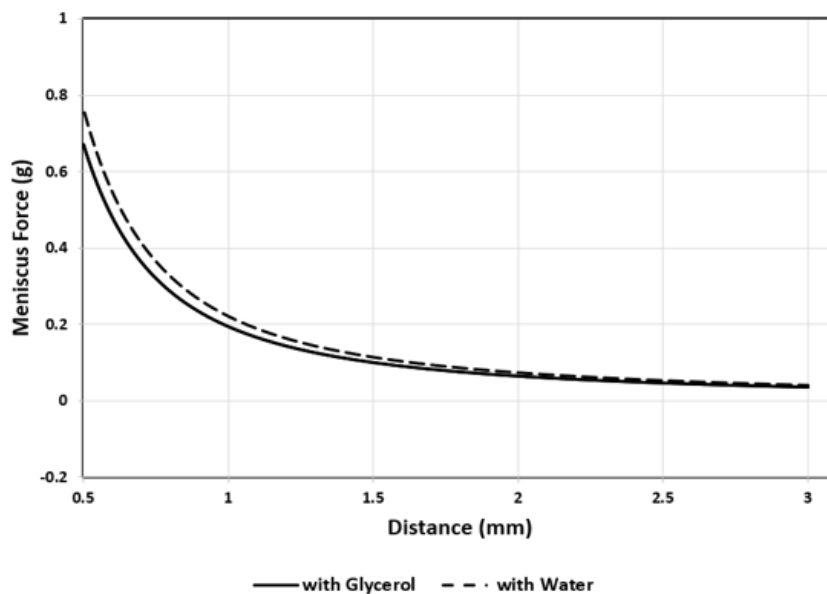


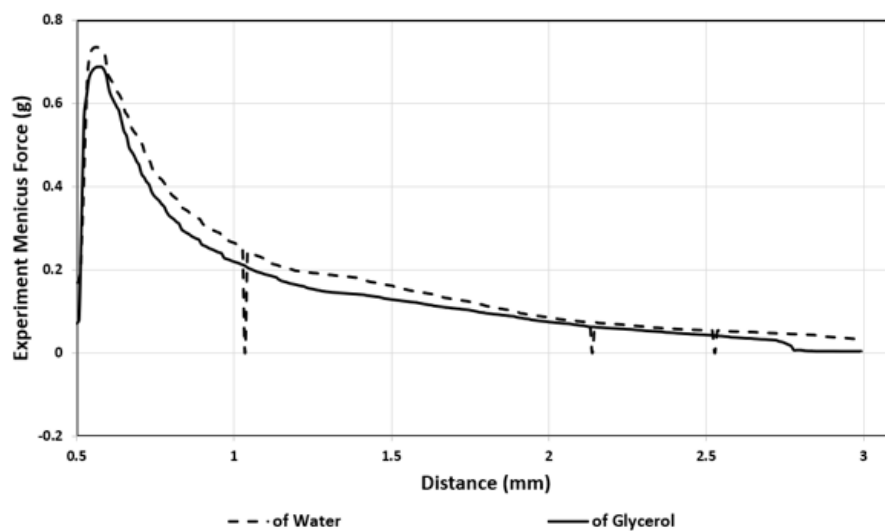
Fig. 47. The theoretical graph for different minimum distances with the same initial conditions for glycerol.

7.3. Comparison of water and glycerol

By using the parameters of glycerol and water in Table. 3, the theoretical meniscus force for water and glycerol is created in Fig. 48a. The experimental meniscus force of glycerol and water with the same surface roughness and parameters in Table. 3 is presented in Fig. 48b.



a)

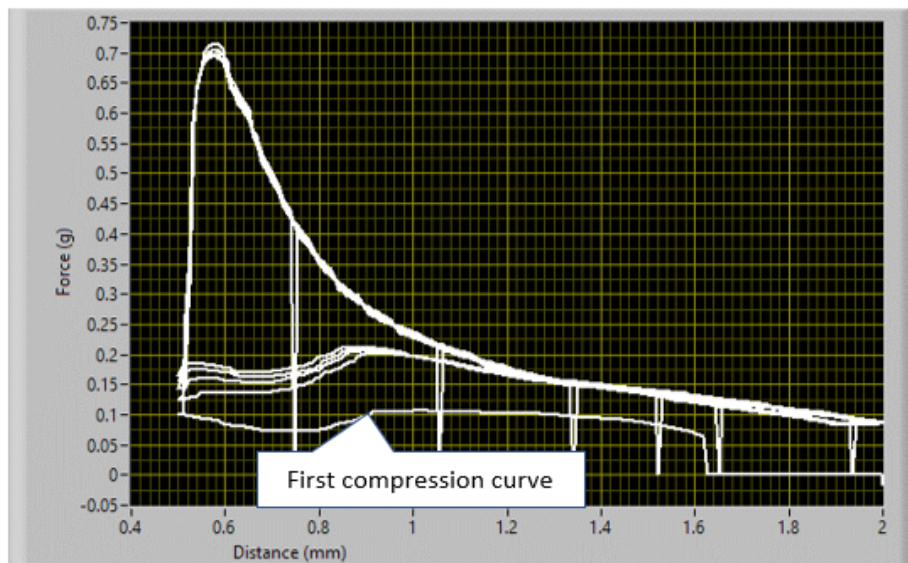


b)

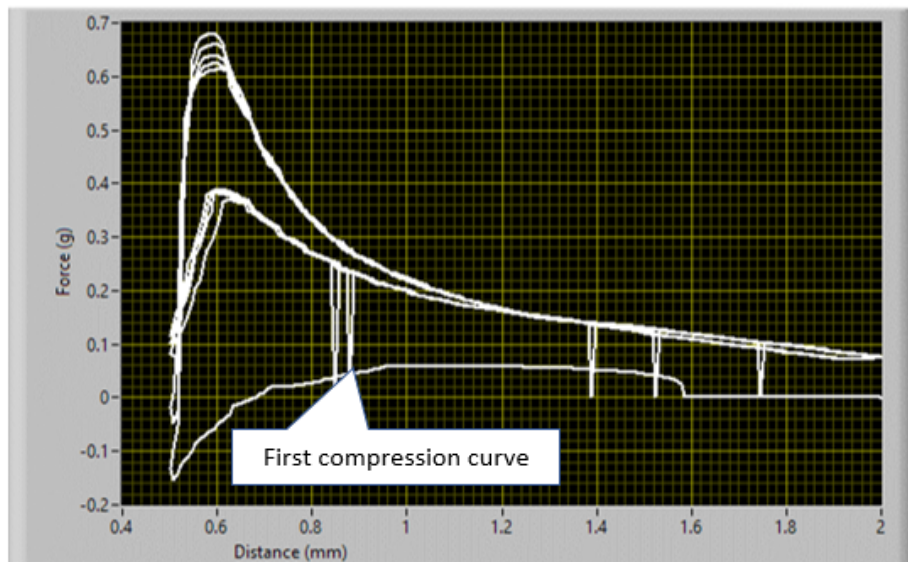
Fig. 48. The theoretical and experimental graph for different liquids with the same roughness and initial volume: a) Theoretical meniscus force for water, glycerol with the parameters listed in Table. 3, b) Experimental meniscus force for water, glycerol with the parameters listed in Table. 3.

In theory, the meniscus force caused by glycerol is smaller than that caused by water with the same configuration. This is because the surface tension of glycerol is smaller than that of water and their receding contact angle is similar. The experimental result is aligned with the theory, but the tolerance of sliding position and the deviation in height of ground surface make the experimental result uncertain. In the experiments of different liquid with the same volume, the maximum separation force reduces with the reduction of surface tension if the receding contact angle is similar.

The cyclic run is conducted to test the repeatability of the system. The experiment includes 5 complete cycles of compression and stretching from the height 2 mm to prevent the break of liquid bridge as shown in Fig. 49. Except for the first compression curve, the force curve repeated in every cycle. This repeated cycle presents the stability of the system. The speed of the slider, the distance and the force measurement are controlled accurately. The exception at the first compression curve is explained by the wetting state of the surface. The wetting state of the surface changes the advancing contact angle. Fig. 49a shows the cyclic run of water on the #240 ground surface, and Fig. 49b shows the cyclic run of glycerol on the same ground surface. The difference of the first compression curve with the other compression curve is shown more obviously in the glycerol experiment. The change of advancing contact angle caused by the wetting status of the surface in glycerol is bigger than that in water. The similar observations are seen in the experiment of water and glycerol with the other surface preparations such as #400, #600.



a)



b)

Fig. 49. Cyclic run experiment of: a) water on the #240 ground surface, b) glycerol on the #240 ground surface

8. Conclusion suggestion for future work

8.1. Conclusion

This study provides real time force measurement in separation process along with the real time image acquisition to explain the deviation between theoretical and experimental methods. The experimental design, setup and initial conditions for experiment are described in detail for further study related to liquid separating force. The simulation model is created to apply the theoretical model in prediction of meniscus force for different initial conditions. The characteristics of solid liquid interface in static and dynamic state are showed in the study with visual demonstration, and how they can affect the experiment results is presented.

The experiments showed that, in the static state, the evaporation will change the geometric parameters such as the contact angle, the vertical radius or the horizontal radius of liquid bridge, and the change of geometric parameters lead to the change of meniscus force. The analytical models also showed that the change of maximum separation force caused by volume or mass deviation and minimum distance deviation is more significant than that caused by contact angle deviation for the liquid with receding contact angle under 40° . The deviation of maximum separation force is not observed in the experiments with different roughness. In the experiments of different liquids with the same volume, the maximum separation force reduces with the reduction of surface tension if the receding contact angle is similar. The experiments results are repeatable and precise in cyclic run. However, the tolerance of sliding position and the deviation in height of ground surface make the experimental results varied in individual run.

8.2. Suggestion for future work

The experimental result is affected largely by the minimum distance which is defined by the tolerance of sliding position and the deviation in height of ground surface. To reduce the deviation of the result, the tolerance of sliding position needs to be reduced by increasing the resolution of the of the motor or changing from open loop to close loop control system. The deviation in height of ground surface can be reduced by designing a grinding tool that utilizes the milling machine to make surface flatter.

The experimental could be conducted with the less hydrophilic surface or with hydrophobic surface to observe how the meniscus force change with larger receding angle. The experiment can be conducted with the same liquid on different surface coating (non-wetting coating, nano-textured surfaces). The experiments with different minimum distances can be conducted to investigate the effect of minimum distance to maximum separation force. The separation velocity can change to verify the effect of viscous force in the total separation force. Experiment can be conducts with the same liquid with different contamination density.

9. References

- [1] S. Cai, B. Bhushan, Meniscus and viscous forces during separation of hydrophilic and hydrophobic surfaces with liquid-mediated contacts, *Materials Science and Engineering R* 61 (2008) 78–106.
- [2] B. Bhushan, *Introduction to Tribology*, John Wiley, New York, 2002.
- [3] I.R. McHaffie, S. Lenher, *J. Chem. Soc.* 127 (1925) 1559–1572.
- [4] J.S. McFarlane, D. Tabor, *Proc. R. Soc. A* 202 (1950) 224–243.
- [5] K.D. Miyoshi, T. Buckley, C. Kusaka, Maeda, B. Bhushan, in: B. Bhushan, N. S. Eiss (Eds.), *Tribology and Mechanics of Magnetic Storage Systems*, ASLE, Park Ridge, IL, 1988.
- [6] L. Wang, R. Weibin, G. Bin, H. Guiming and S. Lining, *Dynamic Separation of a Sphere from a Flat or Sphere in the Presence of a Liquid Meniscus.*, *Tribology Transactions*, 2011.
- [7] V. Popov, *Contact mechanics and friction physical principles and applications*, Heidelberg:Springer, 2010.
- [8] D. Bonn, J. Eggers, J. Indekeu, J. Meunier and E. Rolley, "Wetting and Spreading," *Rev.Mod.Phys*, pp. 739-805, 2009.
- [9] A. Colak, H. Wormeester, H. Zandvliet and B. Poelsema, *Surface adhesion and its dependence on surface roughness and humidity measured with a flat tip*, *Applied Surface Science*, pp. 6938-6942, 2012.

- [10] M. Ataei, T. Tang, A. Amirfazli, Motion of a liquid bridge between nonparallel surfaces, *Journal of Colloid and Interface Science*, Volume 492, 2017, 218-228
- [11] M. Mastrangeli, Q. Zhou, V. Sariolac and P. Lambert, Surface tension-driven self-alignment, *Soft Matter*, 2017, 13, 304
- [12] E. Portuguez, A. Alzina, P. Michaud, D. Hourlier, A. Smith, Study of the Contact and the Evaporation Kinetics of a Thin Water Liquid Bridge between Two Hydrophobic Plates, 2017, 13, 304
- [13] F. Xiao, J. Jing, S. Kuang, L. Yang, A. Yu, Capillary forces on wet particles with a liquid bridge transition from convex to concave, *Powder Technology*, 363, 2020, 59-73
- [14] L. Tadrist, L. Motte, O. Rahli and L. Tadrist, Characterization of interface properties of fluids by evaporation of a capillary bridge, *Royal Society Open Science*, 2019
- [15] Z. Shi, Y. Zhang, M. Liu, D. A. H. Hanaor and Y. Gan, Dynamic contact angle hysteresis in liquid bridges, *Colloids and Surfaces A: Physicochemical and Engineering Aspects*, 2018.
- [16] P. Dhital, Study of Role of Meniscus and Viscous Forces During Liquid-Mediated Contacts Separation, *All Theses, Dissertations and Other Capstone Projects*, 2016, 653.
- [17] D. Saha, *Hydraulics vs Pneumatics - Hydraulic Suspension*, <https://hydraulicsuspension.com/hydraulics-vs-pneumatics/>, 2019

[18] Lifting Systems - LearnEASY,

http://www.learneasy.info/MDME/MEMmods/MEM30009A/lifting_systems/lifting_systems.html

[19] SureStep™ Stepping Systems user manual, STP-SYS-M-WO, 5th Edition, Revision B, 2019.

[20] Big Easy Driver Hookup Guide, TONI_K, Sparkfun,
https://media.digikey.com/pdf/Data%20Sheets/Sparkfun%20PDFs/BigEasyDriverHookupGuide_Web.pdf

[21] OHAUS CORPORATION, EXPLORER ANALYTICAL Instruction Manual,
<https://dmx.ohaus.com/WorkArea/showcontent.aspx?id=28112>

[22] OHAUS CORPORATION, EXPLORER ANALYTICAL datasheet,
<https://dmx.ohaus.com/WorkArea/showcontent.aspx?id=28034>.

[23] H.K.Cammenga, F. W. Schulze, and W. Theuerl, Vapor Pressure and Evaporation Coefficient of Glycerol, Journal of Chemical and Engineering Data, Vol. 22, No. 2, 1977.

[24] R. N. Wenzel, Resistance of Solid Surfaces to Wetting by Water. In: Ind. Eng. Chem. 28, Nr. 8, 1936, S. 988–994

Appendix

Thesis video

The general experimental process

<https://www.youtube.com/watch?v=OZDZdKo-GqM&t=116s>

Experiment of water on the #240 ground surface

<https://www.youtube.com/watch?v=nkn3nI9uWFs>

Simulation of water on the #240 ground surface

<https://www.youtube.com/watch?v=OpEB1PEV8oc>

Cyclic run experiment of water on the #240 ground surface

<https://www.youtube.com/watch?v=lugBUL3HA4c>

Cyclic run experiment of glycerol on the #240 ground surface

<https://www.youtube.com/watch?v=blqVU4XqCX8>

Matlab code

```
%SIMULATION OF LIQUID BRIDGE ONLY
% to run this type the name of script to Matlab command
window
% meniscus_simulation

clear %clear variables in workspace
set(groot, 'defaultLineLineWidth', 1.5)

% initial parameters for meniscus
theta1 = 60; % degree upper contact angle
theta2 = 60; % degree lower contact angle
gamma = 72e-3; % N/m surface tension
```

```

xn0 = 3e-3; % m    initial meniscus radius on horizontal
plane
h0 = 1e-3; % m    initial surface distance
delta = 1e-4; % m iteration distance
ts = 0.1; % second separation time
hs = 14e-3; % breaking distance
eta = 0.89e-3; % Pa.s    dynamic viscosity(1cp = 1e-3
Pa.s)
vec = (hs-h0)/ts

hn_array = [4e-9 6e-9 8e-9 10e-9 12e-9 20e-9 40e-9 60e-
9 80e-9 100e-9 180e-9]; % m    various height
len = length(hn_array);
count = 0;
constR = (cosd(theta1)+cosd(theta2)); % constant from h
to r1

% set the initial value
xn = xn0;
hn = h0;
r1 = hn/constR;

% Calculate initial volume
dd = 1/12*pi*r1;
ee1 = (pi-2*deg2rad(theta1)+sind(2*theta1));
ee2 = (pi-2*deg2rad(theta2)+sind(2*theta2));
ff1 = r1*cosd(3*theta1);
ff2 = r1*cosd(3*theta2);
gg1 = cosd(theta1);
gg2 = cosd(theta2);
aa1 = 12*dd*gg1;
aa2 = 12*dd*gg2;
bb1 = 24*dd*r1*gg1-dd*r1*6*ee1;
bb2 = 24*dd*r1*gg2-dd*r1*6*ee2;
cc1 = 21*dd*gg1*r1^2-dd*r1*ff1 - dd*6*ee1*r1^2;
cc2 = 21*dd*gg2*r1^2-dd*r1*ff2 - dd*6*ee2*r1^2;
aa = aa1+aa2;
bb = bb1+bb2;
cc3 = cc1+cc2;
% The initial volume
V0 = aa*xn^2 + bb*xn +cc3;
cc = cc3-V0;

```

```

% the first moving surface position
linex(1) = xn+r1*(1-sind(theta2));
linex(2) = -linex(1);
liney(1) = hn;
liney(2) = hn;

simu_fig = figure('Name','Liquid
Bridge','NumberTitle','off');
ax = gca; %change the exponent of 10 expressed on axis

% the first meniscus arc position
angleArr = theta1:1:(180-theta2);
arcX = xn + r1 - r1*sind(angleArr);
arcY = r1*cosd(theta1) - r1*cosd(angleArr);

% plot the first meniscus arc and moving surface

%change unit

linex = linex.*10^9;
liney = liney.*10^9;
arcX = arcX.*10^9;
arcY = arcY.*10^9;

plot(linex, liney, '--');
axis([-linex(1) linex(1) 0 4.5*linex(1)]);
hold
plot(arcX, arcY);
plot(-arcX, arcY);
%ax.YAxis.Exponent = -9; %change the exponent of 10
expressed on axis
%ax.XAxis.Exponent = -9;
hold % to keep the curve remove % this hold 1/3
step = 1;
fm(step) = pi*xn^2*gamma/r1 +
2*pi*gamma*xn*sind(theta2);
fv(step) = -3*pi*(xn0^4)*eta*((1/hn^2)-
(1/h0^2))/(4*ts);
dist(step) = hn;

```

```

ylabel('D (nm)');
xlabel('x (nm)');
% Increase the separation distance by delta
while xn > 0 & count < len
    pause(0); % simulation step time
    hn = hn+delta; % uniformly increasing height

    %count = count+1; % eliminate when not use
    variously increasing height
    %hn = hn_array(count); % variously increasing
    height

    r1 = hn/constR;

    % calculate the meniscus radius in horizontal plane
    by constant volume
    dd = 1/12*pi*r1;
    ee1 = (pi-2*deg2rad(theta1)+sind(2*theta1));
    ee2 = (pi-2*deg2rad(theta2)+sind(2*theta2));
    ff1 = r1*cosd(3*theta1);
    ff2 = r1*cosd(3*theta2);
    gg1 = cosd(theta1);
    gg2 = cosd(theta2);
    aa1 = 12*dd*gg1;
    aa2 = 12*dd*gg2;
    bb1 = 24*dd*r1*gg1-dd*r1*6*ee1;
    bb2 = 24*dd*r1*gg2-dd*r1*6*ee2;
    cc1 = 21*dd*gg1*r1^2-dd*r1*ff1 - dd*6*ee1*r1^2;
    cc2 = 21*dd*gg2*r1^2-dd*r1*ff2 - dd*6*ee2*r1^2;
    aa = aa1+aa2;
    bb = bb1+bb2;
    cc3 = cc1+cc2;
    %V0 = aa*xn^2 + bb*xn +cc3;
    cc = cc3-V0;
    xn = max(roots([aa bb cc]));

    % the moving surface position
    liney(1) = hn;
    liney(2) = hn;

    % the meniscus arc position
    angleArr = theta1:1:(180-theta2);

```

```

arcX = xn + r1-r1*sind(angleArr);
arcY = r1*cosd(theta1) - r1*cosd(angleArr);

% plot the meniscus arc and moving surface

%change unit
% lineX not change, so dont change unit
lineY = lineY.*10^9;
arcX = arcX.*10^9;
arcY = arcY.*10^9;

plot(lineX, lineY, '--');
axis([-lineX(1) lineX(1) 0 4.5*lineX(1)]);
hold % to keep the curve remove % this hold 2/3
ylabel('D (nm)');
xlabel('x (nm)');
plot(arcX, arcY);
plot(-arcX, arcY);
%ax.YAxis.Exponent = -9; %change the exponent of 10
expressed on axis
%ax.XAxis.Exponent = -9;
hold % to keep the curve remove % this hold 3/3
step = step+1;
fm(step) = pi*xn^2*gamma/r1 +
2*pi*gamma*xn*sind(theta2);
fv(step) = -3*pi*(xn0^4)*eta*((1/hn^2)-
(1/h0^2))/(4*ts);
dist(step) = hn;

end
ylabel('D (nm)');
xlabel('x (nm)');

pause(0.2);

%plot all the forces
force_fig = figure('Name','Force
Graph','NumberTitle','off');

%fv = -3*pi*(xn0^4)*eta/(4*ts)*((1/hs^2)-(1/h0^2));
%fv_array = fv + zeros(1, step);

```

```

fad = fm+fv;

plot(dist, fm, 'k-
o', 'MarkerIndices', 1:7:length(fm), 'DisplayName', 'Menisc
us force');
xlabel('H (m)');
ylabel('Forces in seperation (N)');
hold
%plot(dist, fad, 'k--
', 'MarkerIndices', 1:7:length(fad), 'DisplayName', 'Total
Adhesive force');
%plot(dist, fv_array, 'k-
x', 'MarkerIndices', 1:7:length(fv_array), 'DisplayName', '
Viscous force at ts = 0.1us');
plot(dist, fv, 'k-
x', 'MarkerIndices', 1:7:length(fv), 'DisplayName', 'Viscous
force at ts = 0.1s');

% plot viscous forces with differrent seperation time
ts1 = 0.001; % second separation time
%fv = -3*pi*(xn0^4)*eta/(4*ts)*((1/hs^2)-(1/h0^2));
%fv_array = fv + zeros( 1, step );
fv = fv*ts/ts1;
plot(dist, fv, 'k-
s', 'MarkerIndices', 1:7:length(fv), 'DisplayName', 'Viscous
force at ts = 0.001s');

ts2 = 0.0001; % second separation time
%fv = -3*pi*(xn0^4)*eta/(4*ts)*((1/hs^2)-(1/h0^2));
%fv_array = fv + zeros( 1, step );
fv = fv*ts1/ts2;
plot(dist, fv, 'k-
d', 'MarkerIndices', 1:7:length(fv), 'DisplayName', 'Viscous
force at ts = 0.0001s');

legend('show');
legend boxoff
hold

```